

# IRN

université paris - sud  
INSTITUT DE PHYSIQUE NUCLEAIRE  
B.P. N° 1 - 91406 - ORSAY - TEL. 941.51.10  
laboratoire associé à l'IN2P3

**SPECTROSCOPIC STUDY OF THE N = 27  
NUCLEI BY MEANS OF THE  $(\tau, \rho)$  REACTION.**

**S. FORTIER, E. HOURANI\*, M.N. RAO\*\* and S. GALES**

**Institut de Physique Nucléaire, B.P. n°1, 91406 Orsay  
France**

**IPNO-PH-N-78-24**

Spectroscopic study of the  $N = 27$  nuclei by means of the  $(\tau, \alpha)$  reaction.

S. FORTIER, E. HOURANI<sup>+</sup>, M.N. RAO<sup>++</sup> and S. GALES  
Institut de Physique Nucléaire, BP n°1, 91406 Orsay, France.

Abstract : The  $(\tau, \alpha)$  reaction on  $^{48}\text{Ca}$ ,  $^{50}\text{Ti}$ ,  $^{52}\text{Cr}$  and  $^{54}\text{Fe}$  target nuclei has been studied at 25 MeV incident energy. Angular distributions have been measured from  $5^\circ$  to  $40^\circ$  with a split-pole spectrometer in a large range of excitation energy. A local zero-range DWBA analysis has been carried out, using an isospin dependent potential for the calculation of the neutron form factor, in order to get a coherent set of spectroscopic factors for both  $T >$  and  $T <$  levels in different nuclei. Assignments of  $l$ -values have been done for a large number of levels, most of them previously unknown, and energy centroids of hole states have been determined. Spectroscopic factors in  $^{39}\text{Ca}$ ,  $^{47}\text{Ti}$ ,  $^{49, 52, 53}\text{Cr}$  have also been obtained for strongly excited states. A sum rule analysis has been carried out for the  $N = 27$  nuclei : the  $1d_{3/2}$  and  $2s_{1/2}$   $T <$  hole strengths are generally fully exhausted by the observed levels, whereas only a fraction of the  $1d_{5/2}$  strength has been evidenced. The  $1f_{7/2}$ ,  $1d_{3/2}$  and  $2s_{1/2}$  analog states have been observed in all nuclei; in  $^{53}\text{Fe}$ , the  $1d_{3/2}$  and  $2s_{1/2}$  analog states appear to be split in several components. In addition, a CRC analysis

---

+ Permanent address : Lebanese University, Faculty of Sciences, Hadat-Beyrouth, Lebanon.

++ Visitor from the University of Sao Paulo, supported by the Fundação de Amparo a Pesquisa do Estado de Sao Paulo.

has been carried out for some levels with angular distributions not accounted for by a direct pick-up process. These levels are tentatively identified with states resulting from the coupling of one  $f_{7/2}$  neutron hole with excited states of the target nucleus. In particular, the  $5/2^-$  and  $9/2^-$  members of the configuration have been identified in each final nucleus; Unambiguous  $J^\pi$  assignments are made; and the two-step  $(\tau, \alpha)$  reaction therefore appears as a useful spectroscopic tool, especially for investigating high spin states.

NUCLEAR REACTIONS  $^{48}\text{Ca}$ ,  $^{48,50}\text{Ti}$ ,  $^{\text{NAT}}\text{Cr}$ ,  $^{54}\text{Fe}$ ,  $(^3\text{He}, \alpha)$ ,  
E = 25 MeV.  $^{47}\text{Ca}$ ,  $^{47,49}\text{Ti}$ ,  $^{49,51,52,53}\text{Cr}$ ,  $^{53}\text{Fe}$  deduced levels,  
 $l$ , J,  $\Pi$ , S; Analog states. DWBA and CRC analyses - Enriched  
targets.

## 1. Introduction.

Hole states in  $f7/2$  shell nuclei have been investigated with a number of different pick-up experiments. However, large discrepancies between the spectroscopic factors determined in different works for the same level are often observed, due to the various experimental conditions and the particular ingredients of the DWBA analysis (optical potentials, different procedure for the calculation of form factors, normalization factors, etc...). Under these conditions, the study of the variation of spectroscopic factors from one nucleus to another, in view of a comparison with theoretical calculations, appears rather difficult. However spectroscopic factors which would be obtained from pick-up reactions realized in the same experimental conditions and analyzed with the same methods would surely be more consistent : in this case the systematic uncertainties which can be attributed to the determination of  $C^2S$  values are expected to be similar for all nuclei studied. The first aim of the present work was to get a coherent set of spectroscopic factors for neutron hole states in the region of the  $N=28$  shell closure. In this paper, we report the results of a systematic study of the  $(\tau, \alpha)$  reaction on  $^{48}\text{Ca}$ ,  $^{50}\text{Ti}$ ,  $^{52}\text{Cr}$  and  $^{54}\text{Fe}$  target nuclei, studied with good energy resolution in a large range of excitation energy. Results obtained in the same work about strong hole levels in  $^{39}\text{Ca}$ ,  $^{47}\text{Ti}$ ,  $^{49,52,53}\text{Cr}$  final nuclei are also reported.

A large amount of data has been obtained in the present work for both  $T<$  and  $T>$  states in nuclei with different neutron excess, and it is therefore possible to study the effect of isospin dependance of the nuclear potential on the determi-

nation of spectroscopic factors : this dependence, although well-established theoretically, is in fact not taken into account in most DWBA analyses.

The present experimental data has been obtained, in general, with better energy resolution and statistics than in the previous (p,d), (d,t) and ( $\tau,\alpha$ ) studies on the same target nuclei<sup>1-4</sup>). Many weak transitions with definite  $l$ -values have been observed for the first time allowing a more accurate determination of centroid energies for the various hole states. Another important point motivating the present study also requires good energy resolution : in the same mass region, analog states of particle levels have been recently observed to be in fact split in two components<sup>5</sup>); the investigation of an eventual splitting of hole analog states in the nuclei studied is therefore of great interest.

Another important spectroscopic interest of the ( $\tau,\alpha$ ) reaction, emphasized in a preliminary report<sup>6</sup>), has been evidenced in the present work and will be presented in section 4. It is shown that  $J^\pi$  assignments can be made for several low-lying levels with non-pick-up angular distributions. For this purpose a coupled reaction channel (CRC) analysis has been carried out, assuming two-step excitation of phonon-hole states due to the coupling of one  $f7/2$  neutron hole with the first  $2^+$  or  $3^-$  level of the target nucleus. The usefulness of the two-step ( $\tau,\alpha$ ) reaction as a spectroscopic tool for investigating high spin states is discussed and direct  $J^\pi$  assignments deduced from the present analysis are compared with those available from  $\gamma$ -ray experiments.

## 2. Experimental procedure.

The  $(\tau, \alpha)$  reaction on  $^{48}\text{Ca}$ ,  $^{50}\text{Ti}$ ,  $^{52}\text{Cr}$ , and  $^{54}\text{Fe}$  target nuclei has been investigated at 25 MeV incident energy with the Orsay MP tandem. The characteristics and isotopic enrichments of the targets are summarized in table 1. The  $\alpha$  particles were detected with silicon position-sensitive detectors (PSD), 700 $\mu\text{m}$  or 1000 $\mu\text{m}$  thick, placed in the focal plane of a split-pole spectrometer. The two outputs E and P from each detector (where E is proportional to the energy lost by the detected particle and P is proportional to E times a function of the particle position along the length of the PSD) were stored on a magnetic tape; identification of  $\alpha$ -particles and calculation of the ratio P/E were done using a Telemecanique T1600 computer. The observed excitation energies extended up to 15 MeV in  $^{47}\text{Ca}$ , using eight PSD in the focal plane. The maximum excitation energies were generally smaller for the other final nuclei (8 MeV or 11 MeV), due to the fact that the study of the  $(\tau, d)$  reaction on the same target nuclei was carried out simultaneously<sup>7-9)</sup> limiting the number of PSD available for the detection of  $\alpha$ -particles. The overall energy resolution for  $\alpha$ -particles was 20-25 keV.

Angular distributions were measured in 5° steps from 5° to 35° lab angle for each target nucleus, and for some of them, additional data were also taken at 40° and 50°. Two successive exposures at different magnetic fields were necessary at each angle in order to cover the spacings between adjacent PSD in the focal plane. The whole  $\alpha$ -spectra were then obtained by juxtaposition of both sets of individual PSD spectra, overlapping each other in a range of 100 to 300 keV. The exci-

tation energies in each final nucleus have been deduced from a calibration of the radius  $\rho$  versus the channel number for each PSD, obtained in a preliminary experiment. This calibration was done by studying the positions of  $\alpha$ -particle with accurately known magnetic rigidity for various values of the magnetic field. Two types of  $\alpha$ -particles have been alternatively used : the 8.78 MeV  $\alpha$ -particles from a ThC source and the  $\alpha$ -peaks corresponding to the ground and two lowest excited states of  $^{57}\text{Ni}$ , produced in the  $^{58}\text{Ni}(\tau, \alpha)^{57}\text{Ni}$  reaction at 25 MeV. The second method, using the accurately known reaction  $Q$ -value<sup>10)</sup> and  $^{57}\text{Ni}$  excitation energies<sup>11)</sup> is expected to give a better precision than the first one, because the energy of the  $\alpha$  particles is close to those of the  $\alpha$ -groups studied in the experiment. Excitation energies in  $^{47}\text{Ca}$  and  $^{47},^{49}\text{Ti}$  have been deduced with an accuracy estimated at about 8 keV, using this method. The energy calibration for the  $(\tau, \alpha)$  reactions on  $^{52}\text{Cr}$  and  $^{54}\text{Fe}$  target nuclei has been obtained using the 8.78 MeV  $\alpha$ -particles : excitation energies in the final nuclei are given with a precision of about 10-15 keV for low-lying levels ( $E_x < 4$  MeV) and 15-20 keV for levels at higher energies.

Absolute cross sections were obtained by comparing the 25 MeV  $^3\text{He}$  scattering data on the various target nuclei with optical model predictions. At these forward angles, theoretical elastic cross sections are very close to the Rutherford predictions, and are almost independent of relatively wide variations of the optical parameters. Independently of statistics, this procedure is estimated to give an overall accuracy of about 15 % for the determination of absolute cross sections.



### 3. Distorted wave analysis.

Experimental data to be analyzed concern a large number of angular distributions obtained in a study of the  $(\tau, \alpha)$  reactions on several  $(f-p)$  shell nuclei. In order to extract from the DWBA analysis coherent spectroscopic information for the whole set of nuclei studied, special care has to be taken for the choice of optical potentials for entrance and exit channels, as well as for the calculation of the bound state form factor. In particular, the existence of an isospin dependent term in the expression of the nucleon-nucleus potential appears to be well established both theoretically and experimentally<sup>12)</sup>, but it is generally not taken into account in conventional DWBA calculations. As the target nuclei studied in this experiment have neutron excess ranging from two to eight, it is necessary to investigate the effect of the isospin - dependence of potential on bound state form factors and theoretical DWBA cross sections. This important point will be examined in section 3.2.

Zero range DWBA calculations have been carried out using the code DWUCK<sup>13)</sup>. In a first step, the form factor for the transferred neutron was calculated using the standard "separation energy procedure" (S.E.) where the depth of the Woods-Saxon well is adjusted in order to reproduce the experimental binding energies. Geometrical parameters of the neutron well are given in table 2. The choice of optical potentials for the entrance and exit channels is now discussed.

### 3.1 - Optical potentials.

Various sets of  $^3\text{He}$  optical parameters obtained from the analysis of elastic scattering data<sup>14)</sup> have been successively used to describe the entrance channel in the DWBA calculation. We have finally adopted an optical potential with real and imaginary depths depending on incident energy and  $\frac{N-Z}{A}$ . This potential proposed by Becchetti and Greenless<sup>15)</sup> reproduce a large amount of scattering data on nuclei with  $A > 40$  and has been found to be well suited for the analysis of the present set of  $(\tau, \alpha)$  experiments.

A large number of  $\alpha$ -particle optical potentials have been obtained from analyses of elastic scattering at various incident energies, on many f.p shell nuclei<sup>14)</sup>. However, attempts to find simple  $E$ - and  $(N-Z)/A$  dependences of the  $\alpha$  potential, similar to those found for  $^3\text{He}$ , were unsuccessful<sup>16)</sup>. We therefore decided to choose an unique  $\alpha$  potential with fixed parameters to describe the exit channels for all the nuclei under study. Only "deep"  $\alpha$ -potentials have been taken into account, in order to fulfil the approximate prescription  $V_\alpha = V_\tau + V_n$ . It has been shown<sup>17)</sup> that this condition is required to ensure the reliability of DWBA in the case of angular momentum mismatch, when the semi-classical momentum  $|K_f - K_i| R$  largely differs from the transferred angular momentum  $l$ ; using this prescription, non locality and finite range corrections appear to be unnecessary. Moreover, the use of a

radial cutoff is not allowed, because the reaction is no more localized to the nuclear surface and partial waves from the nuclear interior may significantly contribute to the reaction, especially in the  $\alpha$ -channel<sup>17)</sup>. Elastic cross sections are not very sensitive to these inner partial waves and the comparison of experimental and theoretical  $(\tau, \alpha)$  angular distribution for transitions with  $\ell$ -mismatch may be taken as a guide in the choice of the "best"  $\alpha$  optical parameters.

Three sets of  $\alpha$  optical potentials, reported in table 2, have been successively used to calculate theoretical angular distributions for some typical transitions in the  $^{48}\text{Ca}(\tau, \alpha)^{47}\text{Ca}$  reaction. The DWBA predictions are compared to the experimental data in fig. 1. One observes that angular distributions are rather well reproduced by the three calculations for different  $\ell$ -values in the case of angular momentum matching ( $\Delta \ell = 0$ ), whereas in the case of mismatch, there are significant differences in the theoretical shapes calculated with the various  $\alpha$ -potentials. The set of optical parameters " $\alpha_A$ " giving the best fit for mismatch transitions has therefore been adopted

### 3.2 - Bound state form factors.

The form factors used in the DWBA analyses are generally calculated using the standard "separation energy method" : the transferred single nucleon wave functions are taken as shell model bound states, calculated in a Woods-Saxon well adjusted to give the experimental binding energy. However this procedure is only approximate when the single particle state is split into several components, and it has been found to give rather poor results in the case of one-neutron pick-up reactions to analog

states in nuclei with large excess of neutrons<sup>19)</sup>. The theoretical cross sections calculated for analog states according to this method are too low compared to the experimental ones, resulting in spectroscopic factors much larger than the shell model sum rules. Stock and Tamura<sup>19)</sup> have shown that the discrepancy is reduced by using an isospin dependent potential in the calculation of the bound state wave function. If a term of the form  $4U_1 \vec{\tau} \cdot \vec{T} / A$  (Lane potential) is added to the usual isoscalar potential  $U_0$ , the wave function  $\psi_{nA}$  that describes the motion of the neutron relative to the analog state is then related to that of the proton coupled to the parent state  $\psi_{pC}$  by the following coupled equations :

$$\left\{ \left( -\frac{\hbar^2}{2m} \Delta - U_0 + V_C - 2 T_+ U_1/A - E_p \right) \psi_{pC} = -2(2T_+)^{1/2} U_1 \psi_{nA}/A \right. \quad (1.1)$$

$$\left\{ \left( -\frac{\hbar^2}{2m} \Delta - U_0 + 2 (T_+^{-1}) U_1/A - E_n \right) \psi_{nA} = -2(2T_+)^{1/2} U_1 \psi_{pC}/A \right. \quad (1.2)$$

In these equations,  $V_C$  is the Coulomb potential,  $A$  the mass of the residual nucleus,  $T_+$  the isospin of the analog state. With neutron form factors obtained by solving these coupled equations, spectroscopic factors are in better agreement with the values expected from sum rule considerations and comparison with spectroscopic factors of parent states<sup>18-20)</sup>. For a coherent analysis of pick-up reactions on several target nuclei with different neutron excess, it appears therefore necessary to take into account the isospin dependance of nuclear potential for calculating form factors. In particular, the effect of the Lane potential on the determination of spectroscopic factors has also to be investigated for levels with

isospin  $T_z = T_y - 1$ , since the wave functions are solutions of the following equation<sup>12)</sup>:

$$\left\{ -\frac{\hbar^2}{2m} \Delta - U_0 + 2T_y U_1/A - E_n \right\} \psi_{nC} = 0 \quad (2)$$

Neutron form factors have been therefore calculated for both  $T_y$  and  $T_z$  states following eqs. (1) and (2). The coupled equations (1) have been solved using code DNUM<sup>21)</sup> and the solutions  $\psi_{nA}$  normalized according to the prescription<sup>19)</sup>

$$\int (\psi_{nA}^2 + \psi_{nC}^2) d\tau = 2T_y + 1 \quad (3)$$

Solutions of eq. (2) have been calculated numerically<sup>22)</sup> and used as form factors for  $T_z$  states. The depth  $U_0$  was adjusted for each state in order to get the experimental binding energy. A surface shape was adopted for the Lane potential

$$U_1(r) = -V_1' a \frac{d}{dr} \left\{ 1 + \exp (r - r_0 A^{1/3})/a \right\}^{-1} \quad (4)$$

where  $r_0$  and  $a$  are respectively equal to 1.25 fm and 0.65 fm. The surface term  $V_1'$  is related to the depth of the equivalent volume potential  $V_1$  by the expression<sup>12)</sup>  $V_1' \approx V_1 r_0 A^{1/3}/2a$ . For all the nuclei studied,  $V_1'$  was taken equal to 90 MeV, corresponding to the usual asymmetry term  $V_1 = 25$  MeV, extracted from elastic scattering and (p,n) experiments<sup>12)</sup>.

Shapes of theoretical angular distributions are identical to those obtained using the standard separation energy method, but their absolute values are found to deviate in a significant way for nuclei with a large excess of neutrons. Ratios of cross sections calculated with and without the Lane potential

for different  $l$ -values are shown in fig.2. The effect of the Lane potential is opposite for  $T_{>}$  and  $T_{<}$  states ; the  $C^2S$  values in  $^{47}\text{Ca}$  are lowered by a factor 1.5 for  $T_{>}$  states and raised by 20-30% for  $T_{<}$  states, which is by no means negligible. The isospin term increases from  $^{53}\text{Fe}$  to  $^{47}\text{Ca}$  and its effect on theoretical cross sections of  $T_{<}$  states also increases. The  $T_{>}$  form factors are solutions of the coupled equations (1.1-1.2) , where the Coulomb energies and isospin-dependent terms both play an important part. With a surface strength  $V_1^s=90$  MeV, the effect of the isospin coupling is perturbed by Coulomb effects and the increase of cross sections for  $1d_{3/2}$  and  $2s_{1/2}$   $T_{>}$  states remains almost the same from  $^{53}\text{Fe}$  to  $^{47}\text{Ca}$ . In the case of the  $1f_{7/2}$  states the coupling term and the Coulomb perturbation are both dominated by the centrifugal term  $l(l+1)/r^2$  and the coupled-channel solution  $\psi_{nA}$  is close to that obtained using the standard separation energy method.

The effect of a variation of 30% of the surface strength  $V_1^s$  has been investigated : it induces a variation of only 5% for spectroscopic factors of  $T_{>}$  states in  $^{48}\text{Ca}$  relative to that obtained at  $V_1^s=90$  MeV. On the other hand, isospin-dependent potential with a volume shape have been found to give no significant effect on the determination of spectroscopic factors compared to those obtained with the separation energy procedure, in agreement with ref.19). In Section 5, spectroscopic factors labelled IDP (isospin-dependent-potential) are deduced from a calculation with a surface potential  $V_1^s=90$  MeV, and compared for each level with those obtained using the separation energy (S.E) method.

Spectroscopic factors for a given  $l$  also depend on the  $j=l\pm 1/2$  value assumed for the levels studied. The differences between theoretical cross sections are about 20% for  $p1/2$  and  $p3/2$ , 40% for  $d3/2$  and  $d5/2$ , 60% for  $f5/2$  and  $f7/2$ . When spin values are unknown, assumptions on  $j$  values have to be made, generally based on shell model arguments; they are given explicitly in tables 6-10. It has been suggested<sup>23)</sup> that the single nucleon form factors could be calculated in a more correct way, by reducing the spin-orbit radius, which is generally taken equal to  $r_0$ . The effect of such a variation is to increase the theoretical cross sections for transitions with  $j=l-1/2$  and decrease them when  $j=l+1/2$ , thus reducing the difference between the spectroscopic factors. This dependence of cross sections relative to the spin orbit radius has been investigated in this work. The change of cross sections for a value of  $r_{so}=1.12$  fm are indicated in table 3. The corrections are generally small for the low  $l$ -values investigated in the present work and will be ignored.

### 3.3. Normalization factor

The  $C^2S$  values are deduced from the theoretical cross section  $\sigma_{DW}^{lj}$  by means of the usual expression

$$C^2S = \frac{2j+1}{N} \frac{\sigma_{exp}^{lj}}{\sigma_{DW}^{lj}} \quad (5)$$

where  $j$  is the total angular momentum of the transferred particle,  $\sigma_{exp}$  the experimental cross section and  $N$  a normalization factor, depending on the overlap of the wave functions of  $^3\text{He}$  and  $\alpha$  particles. Theoretical estimates of  $N$  strongly depend on the form assumed for the  $\alpha$  potential; in the present work, the

normalization factor has been taken equal to the commonly adopted<sup>24)</sup> value of 23. With this normalization factor, the C<sup>2</sup>S value determined using IDP for the <sup>47</sup>Ca ground state exhausts about 90% of the full f7/2 strength, which is quite satisfactory considering the uncertainty of about 20% generally admitted for spectroscopic factors.

#### 4. Coupled reaction channel analysis

As will be shown in Section 5, most experimental angular distributions have been well reproduced with DWBA predictions assuming direct pick-up of one neutron in some definite subshell. However, for a number of low-lying levels in <sup>47</sup>Ca, <sup>49</sup>Ti, <sup>51</sup>Cr and <sup>53</sup>Fe, the observed angular distributions are quite different from those obtained in a direct single-step ( $\tau, \alpha$ ) reaction. Theoretical cross sections due to two-step processes have therefore been calculated and compared to the data.

Coupled reaction channel (CRC) calculations have been performed using code CHUCK<sup>25)</sup>. Optical potentials for the <sup>3</sup>He and  $\alpha$  channels are those used in the DWBA analysis (see table 2). Angular distributions presented in fig.3 have been calculated assuming a ( $\tau, \tau', \alpha$ ) reaction path, involving inelastic scattering of the first 2<sup>+</sup> or 3<sup>-</sup> state of the target nucleus and subsequent pick-up of one neutron in the 1f7/2 subshell. Predictions for two-step excitation of 13/2<sup>-</sup> and 15/2<sup>-</sup> states, proceeding through inelastic excitation of the 4<sup>+</sup> state are also shown in fig.3. It is worth pointing out that these two-step angular distributions are very different from those predicted for a direct pick-up and strongly depend on the J <sup>$\pi$</sup>  value of the



final state. The same characteristic shapes, with  $J^\pi$ -dependence of the angle of first maximum, are also obtained with CRC calculations involving the alternative  $(\tau, \alpha, \alpha')$  mechanism (neutron pick-up in the  $1f7/2$  subshell and subsequent inelastic excitation of the final state by the  $\alpha$ -particle). When direct pick-up is forbidden for spectroscopic reasons, these characteristic  $J^\pi$ -dependent shapes of two-step angular distributions may be experimentally observed. This is just the case for the angular distributions, shown in fig.4, of the well-known  $9/2^-$  levels at 1.16 MeV in  $^{51}\text{Cr}$  and 1.34 MeV in  $^{53}\text{Fe}$ : a direct  $\ell=5$  pick-up is in fact very unlikely, because the occupancy of the  $h9/2$  orbit is expected to be very low in the  $N=28$  target nuclei. That this assumption is quite justified may be seen from the excellent agreement between theoretical and experimental angular distributions.

Interference effects between the  $(\tau, \tau', \alpha)$  and  $(\tau, \alpha, \alpha')$  reaction paths have been calculated assuming weak-coupling model wave functions  $[\lambda \otimes f7/2^{-1}]_J$  for the final levels,  $\lambda$  being the spin of the vibrational level ( $2^+$  or  $3^-$ ) in the target nucleus. This implies that members of a phonon-hole multiplet have the same deformation parameter  $\beta$ , as the one measured for the corresponding state in the target nucleus. The  $\beta$  values used in the calculation are given in table 4. A weight factor  $\sqrt{\frac{2J+1}{3(2\lambda+1)}}$  occurs in the expression of the inelastic scattering amplitude<sup>26)</sup> for the  $(7/2^- \rightarrow J^\pi)$  transition in the final nucleus, as well as in the spectroscopic factor for the  $(\lambda \rightarrow J^\pi)$  pick-up<sup>27)</sup>. The calculations show that about 80% of the absolute cross section is due to the  $(\tau, \alpha, \alpha')$  path.

Based on the good agreement between experimental and theoretical angular distributions,  $J^\pi$  assignments could be proposed without ambiguity for seventeen levels listed in table 5. Their angular distributions are shown in figs.4-6. The  $J^\pi=9/2^-$  assignments previously made for the 1.15 MeV level in  $^{51}\text{Cr}$  and 1.34 MeV level in  $^{53}\text{Fe}$ , based on  $\gamma$ -ray work, are confirmed by the CRC analysis. In addition,  $9/2^-$  is also assigned to the levels at 3.57, 4.71 and 4.92 MeV in  $^{47}\text{Ca}$  and 1.61 MeV in  $^{49}\text{Ti}$ . For the levels at 3.88 MeV in  $^{47}\text{Ca}$ , 1.75 MeV in  $^{49}\text{Ti}$ , 2.00 MeV in  $^{51}\text{Cr}$  and 2.40 MeV in  $^{53}\text{Fe}$ , angular distributions are well fitted assuming a two-step excitation of the  $5/2^-$  member of the  $[2^+ \pi f7/2^{-1}]$  configuration. A  $J^\pi=1/2^+$  assignment is made for the levels at 3.84, 4.39 and 5.05 MeV in  $^{47}\text{Ca}$ . The angular distributions obtained for the levels at 4.53, 4.58 and 4.61 MeV in  $^{47}\text{Ca}$  lead to the respective assignments of  $3/2^+$ ,  $5/2^+$  and  $5/2^+$ : it is to be noted that the two-step character of their angular distributions is not obscured by interference with direct  $l=2$  transfer, which indicates that their spectroscopic factor relative to the  $^{48}\text{Ca}$  ground state is very low.

The CRC differential cross sections shown in figs.4-6 have been multiplied with the normalization factors listed in table 5 in order to fit the data. These factors should be equal to unity for pure weak-coupling states, provided that the  $\beta$ -values used in the calculations are reliable. In particular, the structure of the lowest  $9/2^-$  states in  $^{47}\text{Ca}$ ,  $^{49}\text{Ti}$ ,  $^{51}\text{Cr}$  and  $^{53}\text{Fe}$  nuclei, which lie at almost the same excitation energy as the first  $2^+$  state in the corresponding target nucleus, may be assumed to be mainly  $[2^+ \pi f7/2^{-1}]$ : the normalization factor found for these states in  $^{47}\text{Ca}$ ,  $^{49}\text{Ti}$ ,  $^{51}\text{Cr}$  and  $^{53}\text{Fe}$  are respectively 0.6, 0.4, 0.4 and 1.1, in good agreement with this assumption.

The best fits for the levels at 4.00 and 4.88 MeV in  $^{47}\text{Ca}$  are obtained for  $J^\pi=13/2^-$ , assuming a two-step mechanism involving inelastic excitation of the  $4^+$  state at 4.61 MeV in  $^{48}\text{Ca}$  (see fig.6). However, the normalization factors are too high, especially for the 4.00 MeV level for which  $N$  is equal to 7. Therefore the  $J^\pi=13/2^-$  assignment for this level should be considered tentative, inasmuch as the assumption  $J^\pi=13/2^+$  cannot be rejected: the slopes of the angular distributions at forward angles are very sensitive to interference effects and a good fit with  $J^\pi=13/2^+$  can be obtained when some mixing of  $L=3$  and  $L=5$  inelastic scattering is assumed in the calculation.

For the  $^{53}\text{Fe}$  level at 2.34 MeV, with well-established spin and parity  $11/2^-$ , the angular distribution cannot be fitted assuming a  $[2^+ \otimes f7/2^{-1}]$  structure (see fig.4). This discrepancy between theory and experiment is not well understood and could be due to interference effects not taken into account in the calculation (for example, two-step excitation through higher lying  $2^+$  states in  $^{54}\text{Fe}$ ). The existence of one  $11/2^-$  state in  $^{47}\text{Ca}$  at about 3.6 MeV has been predicted by shell-model calculations<sup>35)</sup>, but no angular distribution with  $11/2^-$  shape similar to the one displayed in fig.3 has been observed in this energy region. It is however worth noticing that the 3.84 MeV level, proposed to have  $J^\pi=7/2^+$  in table 5, has an angular distribution similar to the one measured for the  $11/2^-$  level in  $^{53}\text{Fe}$ . An alternately possible  $J^\pi$  value of  $11/2^-$  for the 3.84 MeV cannot therefore be totally excluded. Such an empirical  $J^\pi$  assignment would however have to be confirmed: (i) by the observation of similar angular distributions for other well-known  $11/2^-$  levels in this mass region, but these levels in  $^{49}\text{Ti}$  and  $^{51}\text{Cr}$  have not

been observed due to the presence of contaminants; (ii) by a CRC calculation using realistic wave functions and taking into account reaction mechanisms neglected in the present analysis.

The angular distribution measured for the lowest  $3/2^-$  state in  $^{47}\text{Ca}$ , which is not correctly fitted assuming a direct  $l=1$  pick-up is also compared in fig.4 with pure two-step predictions. A normalization factor of 0.4 is found, and calculation of interference effects between one- and two-step process using realistic wave functions for the  $2^+$  and  $3/2^-$  states would certainly be of interest. This will not be attempted in the present work.

## 5. Results

The spectroscopic information obtained for all the nuclei studied in the present work is presented in tables 6-10. In this section we only discuss specific points affecting our conclusions as summarized in the tables. Selected results from previous ( $\tau, \alpha$ ) and (p,d) experiments are also given, but an overall comparison of spectroscopic factors previously obtained in the various pick-up reactions at different incident energies<sup>1-4</sup> will not be attempted: it can be however noticed that rather large discrepancies in the  $C^2S$  values are often observed between different works, sometimes due to the choice of the normalization factor for the various pick-up reactions;

Values of  $J$  assumed in the DWBA calculation, if unknown from previous works, have been generally chosen according to shell model prescriptions. For  $l=3$  transitions,  $J$  has been assumed equal to  $7/2$  except for levels strongly excited by stripping reactions but only weakly by pick-up, as the  $1f5/2$  orbit

should be empty in the  $N=28$  target nuclei. For  $\ell=2$  transition,  $J$  has been, in general, assumed equal to  $3/2$ ; however high-lying levels in  $^{47}\text{Ca}$  have been assumed to have  $J^\pi=5/2^+$ , as the  $\ell=2$  summed spectroscopic strength is larger than the  $1d_{3/2}$  sum rule limit. The general discussion about analog states, hole strengths and centroid energies determined in the present work will be given in section 6.

### 5.1. The $^{48}\text{Ca}(\tau, \alpha)^{47}\text{Ca}$ reaction

An  $\alpha$ -particle spectrum recorded at  $15^\circ$  is shown in fig.7. It is obtained by juxtaposition of individual PSD spectra at two magnet exposures, as explained in section 2. Excitation energies of the 112 peaks observed up to 13.5 MeV in  $^{47}\text{Ca}$  are given in table 6. The differential cross sections are typically 10-100  $\mu\text{b}/\text{sr}$ , except for five peaks which largely dominate the spectrum: they correspond to the  $\ell=3$  ground state, the two  $\ell=2$  levels at 2.57 and 13.10 MeV and the two  $\ell=0$  levels at 2.59 and 12.74 MeV. The levels at 12.74 and 13.10 MeV are respectively identified with the analog states of the ground and first excited states of  $^{47}\text{K}$ , carrying the largest part of the  $s_{1/2}$  and  $d_{3/2}$ ,  $T_+$  hole strength. The main components of the  $f_{7/2}$ ,  $d_{3/2}$  ( $T_-$ ) and  $s_{1/2}$  ( $T_-$ ) hole strengths are respectively the levels at 0.0, 2.57 and 2.59 MeV: their spectroscopic factors calculated using the IDP procedure (see §3.2), correspond respectively to 87%, 63% and 78% of the shell model sum rules. Results obtained for the weaker levels are also summarized in table 6.

-  $\ell=3$  levels : Spin and parity  $7/2^-$  has been previously assigned to the 3.42 MeV level<sup>28</sup>). Its angular distribution together with that obtained for the neighbouring level at 3.30 MeV, is compared in fig.7 with  $\ell=3$  and  $\ell=2$  predictions : for these excitation energies, unambiguous discrimination between  $\ell=2$  and  $\ell=3$  assignments is difficult, due to the structureless shapes of both theoretical angular distributions. An  $\ell=3$  assignment is also proposed for some other weakly excited levels (e.g. the 4.78 MeV level with  $J^\pi=5/2^-$ <sup>32</sup>) but the agreement between theoretical and experimental angular distributions is in general rather bad.

-  $\ell=2$  levels : Most levels above 4.9 MeV excitation energies have  $\ell=2$  angular distributions. Examples are shown in fig.7. The cumulative sum of  $C^2S$  values largely exceed the sum rule limit of 3.55 for  $d_{3/2}$  hole states. A large number of these levels may therefore be identified with components of the  $d_{5/2}$  hole state, which appear to be highly fragmented.

-  $\ell=0$  levels : The only  $1/2^+$  levels known from previous experiments were those at 2.57 and 12.74 MeV<sup>32</sup>). In addition to these two states, one level at 5.78 MeV and twelve levels located between 7.8 and 10.8 MeV exhibit  $\ell=0$  angular distributions (see fig.8). These levels have low spectroscopic factors individually, but together carry about 25% of the  $2s_{1/2}$   $T_z$  strength.

- Other levels : About 25 levels in  $^{47}\text{Ca}$  clearly exhibit angular distributions with a non-pick-up (n.p.u.) character. Spin assignments resulting from the CRC analysis and

summarized in table 5 are also included in table 6. Some angular distributions which are not fitted using the simple weak coupling assumptions of section 4 are shown in fig.10. No  $\ell=1$  angular distribution has been observed for the 2.85 level, with previously known<sup>32)</sup>  $J^\pi=(1/2,3/2)^-$ ; it has been suggested<sup>28)</sup> that this level could be a doublet, with a small  $\ell=0$  component: this cannot be excluded by the present data, considering the existence of a minimum at  $10^\circ$ , characteristic of  $\ell=0$  (see fig. 9). In such a case, the spectroscopic factor for the corresponding  $1/2^+$  level would be lower than 0.01.

#### 5.2. The $^{50}\text{Ti}(\tau,\alpha)^{49}\text{Ti}$ reaction.

An  $\alpha$ -particle spectrum observed at  $5^\circ(\text{lab})$  is presented in fig.11. The identification of  $^{49}\text{Ti}$  levels has been made by comparing the  $\alpha$ -particle spectra with one produced in the  $(\tau,\alpha)$  reaction on a natural titanium target; peaks corresponding to other Ti isotopes are also indicated in fig.11. Angular distributions measured for levels up to 8.5 MeV excitation energy are shown in fig.12 with DWBA predictions. The deduced  $C^2S$  values are given in table 7. The level at 8.73 MeV with  $\ell=3$  angular distribution is identified with the analog of the  $^{49}\text{Sc}$  ground state. Levels observed at 10.97 and 11.11 MeV have been identified in previous experiments<sup>34,35)</sup> with the analogs of the  $1/2^+$  and  $3/2^+$  levels at 2.23 and 2.27 MeV in  $^{49}\text{Sc}$ . The  $C^2S$  values given in table 7 for these two levels are only tentative: they have been obtained by normalizing theoretical cross sections to the data at only one angle ( $5^\circ$ ).

Spin and parity  $3/2^-$  had been previously assigned to a level at 1.585 MeV<sup>34)</sup>. Its angular distribution can be however reproduced assuming an  $l=0$  transfer: the existence of a doublet of levels with  $J^\pi=3/2^-$  and  $1/2^+$  can therefore be suggested, as in the case<sup>28)</sup> of the 2.85 MeV peak in  $^{47}\text{Ca}$  (see §5.1). Another explanation would be the excitation of this  $3/2^-$  level by a reaction mechanism other than single-step.

The CRC analysis presented in section 4 has shown that the levels at 1.61 and 1.76 MeV in  $^{49}\text{Ti}$  are excited through double-step processes. The  $5/2^-$  assignment made for the 1.76 MeV level agrees with that deduced from the study of the  $^{47}\text{Ti}(t,p)^{49}\text{Ti}$  reaction<sup>38)</sup>. The 1.61 MeV level is unambiguously identified with the  $9/2^-$  component of the  $[2^+ \otimes f7/2^{-1}]$  multiplet (possible  $J^\pi$  values for this level deduced from previous works<sup>33)</sup> were  $5/2^-$ ,  $7/2^-$  and  $9/2^-$ ). The  $11/2^-$  state, member of the same multiplet, has not been evidenced in the present work: it could be tentatively identified with the  $(5/2^- - 19/2^-)$  level at 1.54 MeV, previously observed in the  $^{50}\text{V}(\tau,\alpha)^{49}\text{Ti}$  reaction<sup>39)</sup>, but here unobserved due to the presence of a contaminant.

### 5.3. The $^{52}\text{Cr}(\tau,\alpha)^{51}\text{Cr}$ reaction.

The  $\alpha$ -particle spectrum obtained at  $15^\circ(\text{lab})$  is displayed in fig.13. Excitation energies of  $^{51}\text{Cr}$  levels, transferred angular momentum and  $C^2S$  values deduced from the DWBA analysis, are given in table 8 and compared with previous pick-up data<sup>40,41)</sup>. The corresponding angular distributions are presented in fig.9. Many new  $l$ -assignments have been done, espe-



cially for weakly excited states. For the strongest levels, the  $C^2S$  values are generally in overall agreement with those found in previous works. Based on their excitation energies and measured  $\ell$ -values, the levels at 6.63, 9.22 and 9.33 MeV have been identified with the analogs of  $^{51}\text{V}$  states, located at 0.0 MeV ( $J^\pi=7/2^-$ ), 2.54 MeV ( $J^\pi=1/2^+$ ) and 2.68 MeV ( $J^\pi=3/2^+$ ).

Some angular distributions with non-pick-up character have also been observed. From the CRC analysis presented in section 4,  $J^\pi$  assignments of  $9/2^-$  and  $5/2^-$  have been respectively made for the levels at 1.15 and 2.00 MeV in agreement with results of  $\gamma$ -ray works<sup>34</sup>). The level at 1.90 MeV has  $J^\pi=3/2^-$ <sup>34</sup>), but its angular distribution shown in fig.9 is badly reproduced with an  $\ell=1$  angular distribution, in contrast with the lowest  $3/2^-$  state at 0.73 MeV: this could give an indication of the existence of some [ $2^+ \otimes f7/2^-$ ] component in the wave function of the 1.90 MeV level, leading to two-step mechanisms interfering with the direct  $p3/2$  pick-up in the  $(\tau, \alpha)$  reaction. The level observed at 2.39 MeV in the present work may tentatively be identified with a known high spin level (probably  $J^\pi=13/2^-$ <sup>3</sup>). However, the corresponding  $\alpha$ -peak is experimentally mixed with a contaminant (an  $\ell=2$  transition from the  $^{54}\text{Cr}(\tau, \alpha)^{53}\text{Cr}$  reaction) and a  $J^\pi$  assignment from the CRC analysis could not be made. Also due to the presence of a contaminant, the angular distribution of the 1.48 MeV level with  $J^\pi=11/2^-$  has not been measured in the present work. Other known  $^{51}\text{Cr}$  levels with high spin values have not been observed due to their very low cross section in the  $(\tau, \alpha)$  reaction: an upper limit of 0.5  $\mu\text{b}/\text{sr}$  is given here for the unobserved 2.26 MeV level, with  $J^\pi=(15/2^-)$ <sup>3</sup>).

#### 5.4. The $^{54}\text{Fe}(\tau, \alpha)^{53}\text{Fe}$ reaction.

Levels observed up to 7.5 MeV excitation energy in  $^{53}\text{Fe}$  are listed in table 9, with their excitation energy and the results of the DWBA analysis. A typical  $\alpha$ -particle spectrum is shown in fig.15 and examples of angular distributions for the various  $\ell$ -transfers observed in this reaction are presented in fig.16.

Levels at 4.26, 7.04 and 7.27 MeV had been identified with respectively the  $1f_{7/2}$ ,  $2s_{1/2}$  and  $1d_{3/2}$  hole analog states in the previous pick-up experiments. In addition, based on their excitation energy, the  $\ell=1$  levels observed in the present experiment at 5.54 and 6.58 MeV can be proposed as analog states of the  $3/2^-$  levels at 1.29 and 2.39 MeV in  $^{53}\text{Mn}$ . However the most striking feature of the present data about  $^{53}\text{Mn}$  analog states is the observation of one  $\ell=0$  level 80 keV below the  $1/2^+$  state at 7.04 MeV and three  $\ell=2$  levels in a 160 keV range around the  $5/2^+$  state at 7.27 MeV. Splitting of isobaric analog states have already been observed in the same mass region<sup>5)</sup>; the present data strongly suggest that the  $s_{1/2}$  and  $d_{3/2}$  analog states are also split in several components. This will be discussed in section 6.

The  $J^\pi=9/2^-$  assignment<sup>4)</sup> previously made for the 1.33 MeV level has been confirmed by the CRC analysis presented in section 4. In addition,  $J^\pi=5/2^-$  is assigned to the previously unknown level at 2.40 MeV, which therefore appears as the  $5/2^-$  member of the  $[2^+_{1/2}f_{7/2}^{-1}]$  configuration. Some non-pick-up angular distributions have also been observed for other  $^{53}\text{Fe}$  levels, but they are not reproduced by the present CRC analysis.

This is in particular the case for the  $11/2^-$  level at 2.34 MeV (see fig.4); it is however of interest to mention that its angular distribution measured in the (p,d) reaction has been well fitted assuming a two-step reaction mechanism<sup>42</sup>).

#### 5.5. Other results.

Some additional data about other  $f7/2$  shell nuclei have been obtained in the present work, due to the presence of other isotopes in the targets (see table 1). They only concern states with important hole strength. The  $C^2S$  values calculated with both SE and IDP procedures are given in table 10 and compared with previous pick-up results.

### 6. Discussion

General trends of the large amount of data obtained in the present work are given in this section. Results of the direct pick-up ( $\tau, \alpha$ ) reaction will be first examined, with special attention to spectroscopic factors of analog states, energy centroids for various ( $l, j$ ) states and summed spectroscopic strengths: particularly their dependence relative to the number of protons in the  $1f7/2$  orbit will be studied. The spectroscopic information about weak coupling states in the  $N=27$  nuclei, extracted from the CRC analysis will be discussed in the last subsection, as well as the necessary conditions for using the two-step ( $\tau, \alpha$ ) reaction as a standard spectroscopic tool.

### 6.1. Analog states.

Excitation energies of the  $1f7/2$ ,  $2s1/2$  and  $1d3/2$  isobaric analog states (IAS) measured in the present experiment and the deduced Coulomb displacement energies relative to the parent states are given in table 11 for all the nuclei studied. The experimental Coulomb energies are compared with the semi-empirical values calculated using the relation<sup>44)</sup>  $\Delta E_C = b_1 (\bar{Z}/A^{1/3}) + b_2$  where  $\bar{Z} = Z_c + \frac{1}{2}$  is the average charge of the isobar pair,  $b_1 = 1430$  keV and  $b_2 = -992$  keV. It can be seen in table 11 that this semi-empirical formula gives values of  $\Delta E_C$  about 100 keV lower than the experimental ones in the case of IAS in the  $N=27$  nuclei.

The spectroscopic strengths of the IAS presented in table 12 have been multiplied by a factor  $(2T_0+1)$ , where  $T_0$  is the isospin of the target nucleus, in order to allow direct comparison with the  $C^2S_p$  values for parent states and shell model predictions. In agreement with most previous studies of pick-up experiments<sup>14-16)</sup>, data presented in table 12 gives evidence that the separation energy method for the calculation of the IAS form factor leads to much too large spectroscopic factors compared with both shell model and  $C^2S_p$  values. Spectroscopic strengths obtained by deducing the IAS form factors from the coupled equations (1.1) and (1.2) are smaller, as it was expected according to fig.2, and therefore in better agreement with the corresponding proton strengths. However the  $f7/2$  spectroscopic factors, although reduced by the IDP procedure still exceed the shell model sum rule by a factor of 1.8, 1.3 and 1.1 for  $^{49}\text{Ti}$ ,  $^{51}\text{Cr}$  and  $^{53}\text{Fe}$  respectively.

This remaining problem about spectroscopic factors of the  $f_{7/2}$  IAS suggests that the true isospin potential could differ from the simple surface potential (with  $V_1^i=90$  MeV,  $r=1.25$  fm,  $a=0.65$  fm) adopted in the present analysis and generally giving good agreement with the previous available data in this mass region<sup>22</sup>). It can be remarked that a surface strength of about 200 MeV with the same geometrical parameters would give  $C^2S$  strengths in agreement with shell model expectation, but in counterpart  $T_{\pm}$  spectroscopic factors would be raised and the summed spectroscopic strengths given in subsection 6.2 would in some cases exceed the shell model sum rules. In conclusion, it appears that the choice of a surface form for the Lane potential allows a better determination of IAS spectroscopic factors; however additional experimental and theoretical investigations would be necessary to get more information about the isospin part of the nuclear potential.

Another fact observed in the present work has to be specially emphasized: the existence of two neighbouring  $l=0$  levels and four  $l=2$  levels in  $^{53}\text{Fe}$  near the expected positions of the  $2s_{1/2}$  and  $1d_{3/2}$  IAS, respectively. The splitting of IAS in  $^{53}\text{Fe}$  can be explained in the following way. These states lie at relatively low energy compared to IAS in other nuclei studied and therefore the  $T_{\pm}$  strength is not fully exhausted (see figs.17-19). In this case, a mixing of the  $T_{\pm}$  state with neighbouring  $T_{\pm}$  levels can occur through the Coulomb potential, giving rise to a splitting of the IAS in several components. The number of components depends only on the density of  $T_{\pm}$  levels with same spin and parity; at low energy, the presence

or absence of neighbouring  $T_{\zeta}$  states is purely accidental. The present data supports this assertion: the  $1d_{3/2}$  and  $2s_{1/2}$  IAS in  $^{53}\text{Fe}$  are split, whereas the  $1f_{7/2}$  IAS appears as a single level, in the limit of the experimental resolution; as for other nuclei with higher isospin, splitting of the IAS is not observed. It can be noticed that other examples of IAS splitting in two components in the same mass region<sup>1)</sup> only concern nuclei with small neutron excess, and therefore small energy difference between  $T_{\zeta}$  and  $T_{\eta}$  energy centroids.

### 6.2. Distribution of neutron-hole strengths.

The distribution of spectroscopic strengths in the  $N=27$  nuclei, for transitions with  $\ell=3, 0$  and  $2$  transferred angular momentum, is displayed in figs. 17-19. One of the striking features is the concentration of the major part of each  $(\ell, j)$ ,  $T_{\zeta}$  strength in one well-isolated level, the other one being the smooth dependence of neutron hole strengths relative to the number of protons in the  $1f_{7/2}$  orbital. In particular, the  $C^2S$  value for the  $1f_{7/2}$  ground state decreases from  $^{47}\text{Ca}$  to  $^{53}\text{Fe}$ , whereas one observes increasing fragmentation of the total  $1f_{7/2}$  strength between several components. One can also point out the smoothly decreasing excitation energies of IAS, due to the  $T_{\zeta}$ -dependence of the isobaric splitting between  $T_{\zeta}$  and  $T_{\eta}$  hole states.

The sums of experimental  $C^2S$  values, calculated with the IDP procedure for all the  $T_{\zeta}$  levels observed in the  $N=27$  nuclei, are reported in table 13 for each  $(\ell, j)$  value and compared to shell-model sum-rule limits. They evidently depend on

the energy range studied, and also on the minimum cross section below which weak transitions are undetected; in this respect, transitions could have been missed in  $^{53}\text{Fe}$ , where the data only concerns levels below 8 MeV, and in  $^{49}\text{Ti}$  due to statistics, which is slightly lower than in other nuclei. Weak transitions at high excitation energy in  $^{51}\text{Cr}$  could also be unobserved due to the background produced by contaminants (carbon, oxygen and other chromium isotopes). The experimental centroid energies  $\sum_i C^2S E_i / \sum_i C^2S_i$  of  $T_{-}$  hole levels, deduced from the present data are given in table 15. The uncertainty on these energies is difficult to estimate, because their determination can be affected by the non-detection of weak transitions, if they are located at high energy: the centroid energies in  $^{47}\text{Ca}$  are therefore probably more reliable than in other nuclei, for the experimental reasons quoted above.

- The  $\lambda=3$  transitions : The summed spectroscopic strengths for all  $\lambda=3$  transitions (except those for known  $5/2^-$  levels) are very close from the shell-model sum rule limit for  $1f7/2$  levels, and the  $1f7/2$  hole strength is therefore probably fully exhausted in the studied energy range for all nuclei. The sum of  $C^2S$  values in  $^{51}\text{Cr}$  slightly exceed the  $1f7/2$  sum rule, suggesting that some of the  $\lambda=3$  levels with assumed  $J^\pi$  value of  $7/2^-$ , could have in fact  $J^\pi=5/2^-$ . Transitions to well known  $5/2^-$  levels have been moreover observed, indicating the presence of  $1f5/2$  neutrons in the target nucleus. The occupation number  $v_j^2 = (\sum C^2S) / (2j+1)$  for the  $1f5/2$  orbital in  $^{52}\text{Cr}$ , deduced from the present experiment, is about 10%. The 1% occupation of the  $1f5/2$  subshell found for  $^{54}\text{Fe}$  is probably under-

estimated: there is very little information about  $1f_{5/2}$  levels in  $^{53}\text{Fe}$  due to the absence of stripping data, and some  $f_{7/2}$  assumptions used in this analysis could be erroneous.

- The  $l=0$  transitions : The  $2s_{1/2}$  summed strengths are in good agreement with the shell model limits (100% for  $^{47}\text{Ca}$  and  $^{51}\text{Cr}$ , about 80% for  $^{49}\text{Ti}$  and  $^{53}\text{Fe}$ ). As it was emphasized in subsection 4.1, a number of very weak  $l=0$  transitions observed above 8 MeV in  $^{47}\text{Ca}$  carry a large part (about 25%) of the total  $2s_{1/2}$  strength. Experimental reasons, as those mentioned above, probably explain the very small number of  $l=0$  levels observed in the three other nuclei.

- The  $l=2$  transitions : The spin values are unknown for most of the observed  $l=2$  levels, and therefore the  $1d_{3/2}$  and  $1d_{5/2}$  states cannot be distinguished in the present sum rule analysis. The largest  $l=2$  summed strength has been found in  $^{47}\text{Ca}$ : it corresponds to the sum of the total theoretical  $1d_{3/2}$  strength and of about 45% of the  $1d_{5/2}$  strength. A part of the  $1d_{5/2}$  strength remains therefore unobserved and could lie above 13 MeV excitation energy. Anyway, the  $1d_{5/2}$  hole strength in  $^{47}\text{Ca}$  appears extremely fragmented, and its centroid energy probably lies above 7 MeV excitation energy. According to the sum rule analysis, the  $1d_{5/2}$  hole strength in  $^{49}\text{Ti}$ ,  $^{51}\text{Cr}$  and  $^{53}\text{Fe}$  is practically not observed in the present experiment.

- The  $l=1$  transitions : A few  $l=1$  transitions have been observed: the summed spectroscopic strengths correspond to an occupation of the  $2p_{3/2}$  orbital of about 1% in  $^{48}\text{Ca}$  and 5% in the three other  $N=27$  nuclei.



### 6.3. Phonon-hole states in the N=27 nuclei.

In each of the four nuclei under study, the CRC analysis has allowed the identification of the  $5/2^-$  and  $9/2^-$  states, resulting from the coupling of one  $1f7/2$  neutron hole with the first  $2^+$  state of the target nucleus, generally described as a one-quadrupole-phonon vibrational state. Other members of the  $[2^+ \otimes 1f7/2^-]$  configuration are  $3/2^-$ ,  $7/2^-$  and  $11/2^-$  states. These states could be the first  $11/2^-$  levels, known from the literature<sup>3,4)</sup> or proposed in section 5, and the second  $3/2^-$  and  $7/2^-$  known levels<sup>1-4)</sup>, located at excitation energies close to that of the corresponding  $2^+$  state. They are presented in fig.14, with the  $9/2^-$  and  $5/2^-$  states evidenced in the present work. The pure weak coupling model predicts degenerate energies for the  $3/2^-$ - $11/2^-$  multiplet; the energy splitting of the different components, which are experimentally observed occur due to configuration mixing. According to the rough estimate of section 4, the intensities of the  $[2^+ \otimes 1f7/2^-]$  configuration in the  $5/2^-$  and  $9/2^-$  wave functions vary between 0.4 and 1, except for the  $5/2^-$  level in  $^{47}\text{Ca}$  with smaller intensity (0.07). In  $^{47}\text{Ca}$ , two other  $9/2^-$  levels have in fact been observed at higher energy (4.71 and 4.92 MeV), with significant  $[2^+ \otimes 1f7/2^-]$  component.

The weak-coupling model also predicts the existence of positive parity states with  $J^\pi = (1/2-13/2)^+$ , obtained by coupling one  $1f7/2$  hole to the  $3^-$  vibrational state of the target nucleus. Such states have been evidenced in  $^{47}\text{Ca}$ , between 3.8 and 5.1 MeV excitation energy, with proposed  $J^\pi$  values  $3/2^+$ ,  $5/2^+$  and  $7/2^+$  (see table 5). However a fragmentation of the pure

$[3^- \pi f7/2^{-1}]$  states occurs: two  $5/2^+$  and three  $7/2^+$  states have been observed, and the ratios of experimental and theoretical cross sections are equal to 0.3 or lower, indicating that their phonon-hole component is rather small. On the other hand, this ratio for the 4.00 MeV level is close to unity, if  $J^\pi=13/2^+$  is assumed, suggesting that this level could be the  $13/2^+$  member of the  $[3^- \pi f7/2^{-1}]$  configuration.

In contrast with  $^{47}\text{Ca}$ , there has been no level with angular distribution characteristic of a  $[3^- \pi f7/2^{-1}]$  structure observed in the three other  $N=27$  nuclei. A simple explanation can be proposed for this fact, in view of the energy difference of the  $2^+$  and  $3^-$  states in the corresponding target nuclei: it is equal to about 3 MeV in  $^{50}\text{Ti}$ ,  $^{52}\text{Cr}$  and  $^{54}\text{Fe}$ , whereas it is only 0.7 MeV in  $^{48}\text{Ca}$ . As the  $1f7/2-1d3/2$  and  $1f7/2-2s1/2$  energy differences between hole states are about 2.5 MeV (see table 14), the positions of the pure weak-coupling  $[2^+ \pi d3/2^{-1}]$  and  $[2^+ \pi s1/2^{-1}]$  configurations are very close to that of the  $[3^- \pi f7/2^{-1}]$  one, in the  $^{49}\text{Ti}$ ,  $^{51}\text{Cr}$  and  $^{53}\text{Fe}$  nuclei. Therefore, a strong mixing of these configurations probably occurs, and interference effects between the different two-step processes, proceeding through inelastic excitation of the  $2^+$  or  $3^-$  states, can destroy the characteristic  $J^\pi$ -dependence displayed in fig.3 for pure  $[3^- \pi f7/2^{-1}]$  states. In  $^{47}\text{Ca}$ , this type of configuration mixing can be expected to be much weaker, at least for low-lying states, as there is a 1.9 MeV energy gap between the unperturbed positions of the configurations involved, and the characteristic shapes predicted by CRC calculations, assuming weak coupling wave functions, are in fact experimentally observed.

In conclusion, the present data shows the power and limits of the proposed method for assigning  $J^\pi$ -values, using the assumption of phonon-hole coupling for analyzing the two-step  $(\tau, \alpha)$  reaction. This method appears very useful, particularly for low-lying high spin states which cannot be excited by direct pick-up for spectroscopic reasons. However, in all the cases where several reaction mechanisms are able to interfere, shapes of angular distributions are no more characteristic of a definite  $J^\pi$  value and a sophisticated CRC analysis using detailed wave functions would then be needed to reproduce the experimental data and test the validity of the structure calculation.

#### 7. Conclusion.

A large amount of new spectroscopic data have been obtained in the present study of the  $(\tau, \alpha)$  reaction. Detailed information about neutron-hole strengths in the  $N=27$  nuclei has been deduced from the observation of many weak transitions with definite angular momentum transfer, up to now unknown. The  $1f7/2$ ,  $2s1/2$  and  $1d3/2$  hole analog states have been studied in all these nuclei, and a splitting of the  $2s1/2$  and  $1d3/2$  IAS has been evidenced in  $^{53}\text{Fe}$ . Finally, in each nucleus, some levels have been excited by the  $(\tau, \alpha)$  reaction through two-step mechanisms, as demonstrated by the present coupled-reaction channel analysis. The assumption of phonon-hole coupling used in this analysis has been fully justified by the good agreement between the theoretical and the experimental angular distribu-

tions and has allowed many direct  $J^\pi$  assignments, most of them for previously unknown levels. The two-step  $(\tau, \alpha)$  reaction appears therefore very useful for investigating phonon-hole states, giving additional motivation for spectroscopic studies using the  $(\tau, \alpha)$  reaction. An extension of the present study to other (f-p) shell nuclei would surely be of interest. An analysis of the  $^{58}\text{Ni}(\tau, \alpha)^{57}\text{Ni}$  reaction, performed in the same experimental conditions, is now in progress<sup>47)</sup>.

We wish to thank Drs H.Laurent, J.M. Maison and J.P.Schapira for their aid in the data taking and Miss F.Samaran for her assistance with the computer codes used in the data analysis. The help of Mrs M.Dormeau, J.Rouvet, D.Bonneau and J.Leterrier in preparing the manuscript and drawings is gratefully appreciated. The operating crew of the Orsay tandem is also acknowledged for the efficient running of the accelerator.

## References

- 1) M.L.Halbert, Nuclear Data Sheets 22 (1977) 59
- 2) S.Raman, Nuclear Data Sheets 4 (1970) 397
- 3) M.N.Rao and J.Rappaport, Nuclear Data Sheets B3-5,6 (1970) 37
- 4) R.L.Auble, Nuclear Data Sheets 21 (1977) 323
- 5) J.P.Schapira, J.M.Maison, N.M.Rao, S.Fortier, S.Galès, and H.Laurent, Phys. Rev. C17 (1978) and refs. therein.
- 6) S.Fortier and S.Galès, Phys. Lett. B, to be published
- 7) S.Galès, S.Fortier, H.Laurent, J.M.Maison and J.P.Schapira, Nucl. Phys. A259 (1976) 189
- 8) S.Galès, S.Fortier, H.Laurent, J.M.Maison and J.P.Schapira, Phys. Rev. C14 (1976) 842
- 9) S.Fortier, J.M.Maison, S.Galès, H.Laurent and J.P.Schapira, Nucl. Phys. A288 (1977) 82
- 10) A.H.Wapstra and N.B.Gove, Nuclear Data Tables 9 (1971) 265.
- 11) R.L.Auble, Nuclear Data Sheets 20 (1977) 327
- 12) G.R.Satchler, in Isospin in Nuclear Physics, ed. D.H.Wilkinson (North Holland, Amsterdam, 1969) p.391
- 13) P.D.Kunz, University of Colorado, report C00-535-606
- 14) C.M.Perey and F.G.Perey, Nuclear Data Tables 17 (1976) 1
- 15) F.D.Becchetti Jr. and G.W.Greenless, in Polarization Phenomena in Nuclear Reactions (H.H.Barschall and W. Haeberli, eds) The University of Wisconsin Press, Madison Wis. (1971) 682
- 16) O.F.Lemos, Thèse de Doctorat de l'Université, Orsay (1972) unpublished
- 17) R.Stock, B.Bock, P.David, H.H.Duhm and T.Tamura, Nucl. Phys. A104 (1967) 136
- 18) L. McFadden and G.R.Satchler, Nucl. Phys. 84 (1966) 177
- 19) R.Stock and T.Tamura, Phys. Lett. 22 (1966) 304
- 20) S.Galès, E.Hourani, S.Fortier, H.Laurent, J.M.Maison and J.P.Schapira, Nucl. Phys. A288 (1977) 201

- 21) M.Beiner and P.Gara, *Comp. Phys. Comm.* 4 (1972) 1
- 22) E.Hourani, private communication
- 23) B.H.Wildenthal, E.Newman, R.L.Auble, *Phys. Rev.* C3 (1971) 1199
- 24) P.M.Endt, *Atomic Data and Nucl. Data Tables* 19 (1977) 23
- 25) P.D.Kunz, Computer code CHUCK, University of Colorado, private communication
- 26) A.Bohr and B.R.Mottelson, in *Nuclear Structure*, ed. W.A.Benjamin (1975) vol.II
- 27) G.R.Satchler, *Ann. Phys.* 3 (1958) 275
- 28) C.R.Gruhn, T.Y.Kuo, C.J.Maggiore and B.M.Preedom, *Phys. Rev.* C6 (1972) 946
- 29) R.L.Auble, *Nuclear Data Sheets* 19 (1976) 291
- 30) J.Rappaport, *Nuclear Data Sheets* B3-5,6 (1970) 1
- 31) H.Verheul, *Nuclear Data Sheets* B3-5,6 (1970) 85
- 32) M.E.Williams-Norton and R.Abegg, *Nucl. Phys.* A291 (1977) 429
- 33) V.K.Rasmussen, *Phys. Rev.* C13 (1976) 631
- 34) R.L.Auble, *Nuclear Data Sheets* 23 (1978) 163
- 35) G.Sartoris and L.Zamick, *Phys. Rev.* 167 (1968) 1035
- 36) D.D.Borlin, Thesis, Washington University (1967)
- 37) P.J.Plauger and E.Kashy, *Nucl. Phys.* A152 (1970) 609
- 38) A.E.Ball, G.Brown, A.Denning and R.N.Glover, *Nucl. Phys.* A183 (1972) 472
- 39) S.A.Andersen, O.Hansen, L.Vistissen, R.Chapman and S.Hinds, *Nucl. Phys.* A125 (1969) 65
- 40) C.A.Whitten Jr. and L.C.McIntyre, *Phys. Rev.* 160 (1967) 997
- 41) P.David, H.H.Duham, R.Bock and R.Stock, *Nucl. Phys.* A128 (1969) 47
- 42) R.O.Nelson and N.R.Robertson, *Phys. Lett.* 43B (1973) 389
- 43) P.Martin, M.Buenerd, J.Dupont and M.Chabre, *Nucl. Phys.* A185 (1972) 465
- 44) J.Janecke, *Isospin in Nuclear Physics*, ed. D.H.Wilkinson (North-Holland Amsterdam, 1969)

- 45) E.Newman and J.C.Hiebert, Nucl. Phys. A110 (1968) 366
- 46) D.Fachner, R.Santo, H.H.Duhm, R.Bock, and S.Hinds, Nucl. Phys. A106  
(1968) 577
- 47) S.Fortier and S.Galès, to be published .

### Figure captions

- Fig.1. DWBA predictions, using three different sets of optical potentials for the  $\alpha$ -particle channel, compared with experimental angular distributions in the  ${}^4\text{He}(\tau, \alpha){}^47\text{Ca}$  reaction, in the case of angular momentum matching ( $\Delta l \approx 0$ ) or mismatch ( $\Delta l \neq 0$ ).
- Fig.2. Ratio of theoretical  $(\tau, \alpha)$  cross sections  $\sigma_{\text{IDP}}/\sigma_{\text{SE}}$  for  $T_>$  and  $T_<$  hole states in the  $N=27$  nuclei. The neutron form factor used in the determination of  $\sigma_{\text{SE}}$  has been calculated with the usual separation energy procedure; as for  $\sigma_{\text{IDP}}$ , an isospin-dependent potential with  $V_1^{\pm} = 90$  MeV has been used in the form factor calculation.
- Fig.3. Shapes of CRC angular distributions for various  $J^{\pi}$  states. The reaction paths assumed in the calculation are drawn in the figure.
- Fig.4. Comparison of experimental angular distributions and CRC calculations assuming a pure  $[2^{+} \otimes f7/2^{-1}]$  structure for final states (solid line). The dashed lines are predictions assuming excitation through the  $(\tau, \tau', \alpha)$  path only. Normalization factors are indicated in table 5.
- Fig.5. Comparison of experimental angular distributions and CRC calculations assuming a pure  $[3^{-} \otimes f7/2^{-1}]$  structure for final states (solid line). The dashed lines are predictions assuming excitation through the  $(\tau, \tau', \alpha)$  path only. Normalization factors are indicated in table 5.



- Fig.6. Comparison of experimental angular distributions with CRC predictions for the  $13/2^+$  member of the  $[4^+ \text{f} 7/2^{-1}]$  configuration (solid line). Shapes of angular distributions calculated in the case of only one  $(\tau, \tau', \alpha)$  reaction path are also indicated (dashed lines). The dotted lines are predictions for a  $[3^- \text{f} 7/2^{-1}]$  state with  $J^\pi = 13/2^-$ . Normalization factors are indicated in table 5.
- Fig.7. The  $\alpha$ -spectrum from the  $^{48}\text{Ca}(\tau, \alpha)^{47}\text{Ca}$  reaction at  $15^\circ$  (lab), observed in the focal plane of the split-pole spectrometer. The numbers on the top of the peaks refer to  $^{47}\text{Ca}$  levels, reported in table 6.
- Fig.8. Examples of angular distributions with  $\ell=2$  angular momentum transfer. For the levels at 3.30 and 3.42, both  $\ell=2$  and  $\ell=3$  DWBA predictions are shown for comparison.
- Fig.9. Examples of  $\ell=0$  angular distributions and comparison with DWBA predictions.
- Fig.10. Examples of angular distributions with non-pick-up character.
- Fig.11. The  $\alpha$ -spectrum from the  $^{48}\text{Ti}(\tau, \alpha)^{47,49}\text{Ti}$  reaction at  $5^\circ$  (lab), observed in the focal plane of the split-pole spectrometer. Peaks labelled with bare numbers correspond to  $^{49}\text{Ti}$  levels reported in table 7. Peaks labelled with primed numbers correspond to  $^{47}\text{Ti}$  levels (see table 10).

- Fig.12. Experimental angular distributions and DWBA predictions in the  $^{50}\text{Ti}(\tau,\alpha)^{49}\text{Ti}$  reaction.
- Fig.13. The  $\alpha$ -spectrum from the  $(\tau,\alpha)$  reaction on a natural chromium target, observed at  $15^\circ$  (lab) in the focal plane of a split-pole spectrometer. Numbers on the top of the peaks correspond to  $^{51}\text{Cr}$  levels, reported in table 8. Peaks identified with levels from other chromium isotopes are labelled explicitly. The large peaks below peaks n $^\circ$ 21,44,49 are contaminants.
- Fig.14. Experimental angular distributions and DWBA predictions in the  $^{52}\text{Cr}(\tau,\alpha)^{51}\text{Cr}$  reaction.
- Fig.15. The  $\alpha$ -spectrum from the  $^{54}\text{Fe}(\tau,\alpha)^{53}\text{Fe}$  reaction, observed at  $15^\circ$  (lab) in the focal plane of a split-pole spectrometer. Numbers on the top of the peaks correspond to  $^{53}\text{Fe}$  levels, reported in table 9.
- Fig.16. Experimental angular distributions and DWBA predictions in the  $^{54}\text{Fe}(\tau,\alpha)^{53}\text{Fe}$  reaction.
- Fig.17. Experimental distribution of the  $f7/2$  strength. Centroid energies of  $T_c$  states are indicated with arrows.
- Fig.18. Experimental distribution of the  $2s1/2$  strength.
- Fig.19. Experimental distribution of the  $1d3/2$  and  $1d5/2$  strengths.

Fig.20. Energies of the levels proposed as members of the  $[2^+ \text{f}7/2^{-1}]$  configuration in the N=27 nuclei, compared to the energy of the corresponding  $2^+$  state. The J values given within parentheses are only tentative. Spin assignments are from the literature for  $3/2^-$ ,  $7/2^-$  and  $11/2^-$  levels, and from the present work for  $5/2^-$  and  $9/2^-$  levels.

**Table 1.** Characteristics of the targets.

Target	$^{48}\text{Ca}$ <sup>a)</sup>	$^{48}\text{Ti}$ - $^{50}\text{Ti}$ <sup>b)</sup>	$^{52}\text{Cr}$ <sup>c)</sup>	$^{54}\text{Fe}$ <sup>b)</sup>
Isotopic enrichment (%)	97.2%	30.7%-57.8%	83.8%	96.8%
Thickness ( $\mu\text{g}/\text{cm}^2$ )	0.35	0.25	0.10	0.10

a) obtained by evaporation onto a  $10 \mu\text{g}/\text{cm}^2$  carbon foil.

b) self-supporting metal foil.

c) natural chromium, evaporated onto a thin formvar backing.

Table 2. Optical model parameters<sup>a)</sup> used in the distorted wave calculations.

Particle	$V_0$ (MeV)	$r_0$ (fm)	$a_0$ (fm)	$W$ (MeV)	$r_i$ (fm)	$a_i$ (fm)	$V_1^i$ (MeV)	$r_c$ (fm)
n	$U_0$	1.25	0.65	-	-	-	0. or 90.	-
$^3\text{He}$ b)	$V_{BG}$	1.20	0.72	$W_{BG}$	1.40	0.88	-	1.3
$\alpha$ {	set $\alpha_A$ c)	206.3	1.37	25.1	1.37	0.56	-	1.4
	set $\alpha_B$ d)	198.6	1.458	19.9	1.458	0.502	-	1.3
	set $\alpha_C$ c)	211.0	1.14	28.8	1.14	0.75	-	1.3

a) The potentials for  $^3\text{He}$  and  $\alpha$  were of the form :

$$V(r) = V_c - V_0 f(r, r_0 A^{1/3}, a_0) - iW f(r, r_i A^{1/3}, a_i)$$

where  $f(r, r_0 A^{1/3}, a_0) = 1/[1 + \exp\{(r - r_0 A^{1/3})/a_0\}]$ , and  $V_c$  is the Coulomb potential. The form factors are computed with a binding potential :

$$U(r) = -U_0 \left[ f(r, r_0 A^{1/3}, a_0) - \frac{\lambda \vec{L} \cdot \vec{S}}{45.2} \frac{1}{r} \frac{d}{dr} f(r, r_0 A^{1/3}, a_0) \right] + (4U_1/A) \vec{\tau} \cdot \vec{I}$$

where the isospin dependent potential is of the form

$$U_1 = -V_1^i a_0 \frac{d}{dr} f(r, r_0 A^{1/3}, a_0) \quad \text{and} \quad V_1^i = 90 \text{ MeV} \quad , \lambda = 25.$$

b) Ref. 15) ; the depths are  $V_{BG} = 151.9 - 0.17 E + 50\xi$  ;  $W = 41.7 - 0.33 E + 44\xi$  where  $E$  is the incident energy in MeV and  $\xi$  is equal to  $(N-2)/A$ .

c) Ref. 16).

d) Ref. 18).

**Table 3.** Mean values of the ratio of theoretical ( $r, \alpha$ ) cross sections calculated with two different spin-orbit radii :  $r_{so} = 1.12$  fm and  $r_{so} = 1.25$  fm.

$l$	$\sigma(r_{so} = 1.12) / \sigma(r_{so} = 1.25)$	
	$l - \frac{1}{2}$	$l + \frac{1}{2}$
1	1.07	0.97
2	1.11	0.94
3	1.16	0.89

**Table 4.** Excited states of target nuclei involved in the CRC analysis of the two-step ( $\tau, \alpha$ ) reaction.

Target Nucleus	$J^\pi$	$E_x$ (MeV)	$\beta$
$^{48}\text{Ca}$	$2^+$	3.83	0.16 <sup>a)</sup>
	$3^-$	4.50	0.18 <sup>a)</sup>
	$4^+$	4.61	0.05 <sup>a)</sup>
$^{50}\text{Ti}$	$2^+$	1.55	0.18 <sup>b)</sup>
$^{52}\text{Cr}$	$2^+$	1.43	0.19 <sup>c)</sup>
$^{54}\text{Fe}$	$2^+$	1.41	0.17 <sup>d)</sup>

<sup>a)</sup> Ref. 28).    <sup>b)</sup> Ref. 29).    <sup>c)</sup> Ref. 30).    <sup>d)</sup> Ref. 31).

Table 5 : Results of the CRC analysis.

final nucleus	$E_x$ (MeV)	$J^\pi$ a)	Assumed configuration	$N^b)$	Previous results	
					$E_x$	$J^\pi$
$^{42}\text{Ca}$	3.57	$9/2^-$	$2^+ \# f7/2^{-1}$	0.6 (2.6)	3.57 <sup>c)</sup>	
	3.84	$7/2^+$	$3^- \# f7/2^{-1}$	0.3 (2.0)		
	3.88	$5/2^-$	$2^+ \# f7/2^{-1}$	0.07(0.4)	3.88 <sup>c)</sup>	
	4.00	$(13/2^-)$	$4^+ \# f7/2^{-1}$	7 (34)		
		$(13/2^+)$	$3^- \# f7/2^{-1}$	0.7 (3.8)		
	4.39	$7/2^+$	$3^- \# f7/2^{-1}$	0.2 (1.6)		
	4.53	$3/2^+$	$3^- \# f7/2^{-1}$	0.08(0.2)		
	4.58	$5/2^+$	$3^- \# f7/2^{-1}$	0.06(0.3)		
	4.61	$5/2^+$	$3^- \# f7/2^{-1}$	0.2 (1.0)		
	4.71	$9/2^-$	$2^+ \# f7/2^{-1}$	0.1 (0.06)		
	4.88	$13/2^-$	$4^+ \# f7/2^{-1}$	3 (12)		
	4.92	$9/2^-$	$2^+ \# f7/2^{-1}$	0.05(0.3)		
	5.05	$7/2^+$	$3^- \# f7/2^{-1}$	0.06(0.5)		
	$^{43}\text{Ti}$	1.61	$9/2^-$	$2^+ \# f7/2^{-1}$	0.4 (2.3)	1.62
1.76		$5/2^-$	$2^+ \# f7/2^{-1}$	0.6 (2.6)	1.76	$5/2^-$ d)
$^{51}\text{Cr}$	1.15	$9/2^-$	$2^+ \# f7/2^{-1}$	0.4 (2.2)	1.16	$9/2^-$ e)
	2.00	$5/2^-$	$2^+ \# f7/2^{-1}$	0.6 (3.0)	2.00	$(5/2)^{-e}$
$^{53}\text{Fe}$	1.33	$9/2^-$	$2^+ \# f7/2^{-1}$	1.1 (5.7)	1.33	$9/2^-$ f)
	2.34	$(11/2^-)$	$2^+ \# f7/2^{-1}$	0.2 (0.9)	2.34	$11/2^-$ f)
	2.40	$5/2^-$	$2^+ \# f7/2^{-1}$	0.4 (1.3)		

a) Proposed based on the CRC analysis

b) Ratio of experimental to theoretical cross sections. The numbers within parentheses are calculated assuming that only the  $(\tau, \tau', \alpha)$  reaction path occurs

c) ref<sup>32)</sup> d) ref<sup>33)</sup> e) ref<sup>34)</sup> f) ref<sup>35)</sup>



Table 6 : Results of the  $^{48}\text{Ca}(\tau,\alpha)^{47}\text{Ca}$  reaction.

n° a)	This work				Previous results <sup>e)</sup>					
	E <sub>x</sub> (MeV)	ℓ	J <sup>π</sup> c)	C <sup>2</sup> S (SE) (IDP)	E <sub>c</sub> (MeV)	(±keV)	ℓ	(p,d)	C <sup>2</sup> S (d,t)	(τ,α)
1	0.0	3	7/2 <sup>-</sup>	5.42 6.94	0.0		3	6.7	6.22	7.76
2	2.014	(1)	3/2 <sup>-</sup>	0.03 9.04	2.014	(2)	1	(0.02)	0.10	0.09
3	2.569	2	3/2 <sup>+</sup>	1.74 2.23	2.578	(4)	2	3.6	1.18	3.4
4	2.591	0	1/2 <sup>+</sup>	1.08 1.38	2.599	(4)	0	1.8	1.28	1.77
5	2.846	n.p.u			2.849	(5)	1			
6	3.267	(3)	(7/2 <sup>-</sup> )	0.01 0.02						
7	3.296	(3)	(7/2 <sup>-</sup> )	0.03 0.04	3.315	(15)	3	0.03		
8	3.423	(3)	(7/2 <sup>-</sup> )	0.10 0.13	3.425	(5)	3	0.07	0.21	0.11
9	3.566	n.p.u	CRC: 9/2 <sup>-</sup>		3.575	(15)				
10	3.844	n.p.u	CRC: 7/2 <sup>+</sup> (or 1/2 <sup>-</sup> )							
11	3.877	n.p.u	CRC: 5/2 <sup>-</sup>		3.872	(15)				
12*	3.933	(3)	(7/2 <sup>-</sup> )	0.06 0.08	3.944	(15)	3			0.08
13	3.997	n.p.u	CRC: (13/2 <sup>+</sup> )		4.019	(5)	1			0.02
14	4.050	(1)	(1/2 <sup>-</sup> )	0.01 0.01	4.058	(3)	1			
15	4.102	(2)	(3/2 <sup>+</sup> )	0.03 0.05	4.103	(5)	(2)			0.08
16	4.205	4	(9/2 <sup>+</sup> )	0.01 0.01	4.202	(15)	3			0.02
17*	4.386	n.p.u	CRC: 7/2 <sup>+</sup>							
17 <sub>B</sub>	4.412	n.p.u			4.402	(5)	1			0.04
18	4.455	n.p.u								
19	4.531	n.p.u	CRC: 3/2 <sup>+</sup>							
20	4.584	n.p.u	CRC: 5/2 <sup>+</sup>							
21	4.611	n.p.u	CRC: 5/2 <sup>+</sup>		4.600	(20)				
22	4.714	n.p.u	CRC: 9/2 <sup>-</sup>							
23	4.785	(3)	(5/2 <sup>-</sup> )	0.01 0.01	4.785	(5)	3			0.05
24	4.810	n.p.u			4.809	(3)	1			
25	4.880	n.p.u	CRC: 13/2 <sup>-</sup>							
26	4.918	n.p.u	CRC: 9/2 <sup>-</sup>							
27	4.960	2	(5/2 <sup>+</sup> )	0.02 0.03						
28	4.980	2	(5/2 <sup>+</sup> )	0.14 0.20	4.989	(15)	2	0.22		0.16
29	5.053	n.p.u	CRC: 7/2 <sup>+</sup>							
30*	5.189	n.p.u			5.289	(5)	1			
31	5.245	2	(5/2 <sup>+</sup> )	0.01 0.01	5.254	(5)				
32	5.293	2	(5/2 <sup>+</sup> )	0.08 0.12	5.305	(5)	2	0.17		0.08



Table 6 (continued)

n <sup>a</sup> )	E <sub>x</sub> <sup>b)</sup> (MeV)	This work			Previous results e)						
		ℓ	J <sup>π</sup> c)	C <sup>2</sup> S (SE) (IDP)	E <sub>x</sub> (MeV)	(± keV)	ℓ	(p,d)	C <sup>2</sup> S (d,t)	(τ,α)	
67	7.842	n.p.u									
68	7.893	0	1/2 <sup>+</sup>	0.03 0.04							
		+									
		2	(5/2) <sup>+</sup>	0.01 0.02							
69	7.954	2	(5/2) <sup>+</sup>	0.03 0.04							
70	7.995	n.p.u									
71	8.021	0	1/2 <sup>+</sup>	0.02 0.03							
72	8.121	0	1/2 <sup>+</sup>	0.02 0.03							
73	8.264	(3)									
74	8.301	2	(5/2) <sup>+</sup>	0.03 0.04							
75	8.352	2	(5/2) <sup>+</sup>	0.02 0.04							
76	8.380	0	1/2 <sup>+</sup>	0.04 0.05							
77	8.447										
78*	8.595	0	1/2 <sup>+</sup>	0.01 0.01							
		+									
		2	(5/2) <sup>+</sup>	0.01 0.02							
79*	8.669	0	1/2 <sup>+</sup>	0.01 0.01							
		+									
		2	(5/2) <sup>+</sup>	0.03 0.04							
80*	8.748	0	1/2 <sup>+</sup>	0.01 0.01							
		+									
		2	(5/2) <sup>+</sup>	0.02 0.03							
81	8.902										
82	8.995										
83	9.124	0	1/2 <sup>+</sup>	0.02 0.03							
84	9.230	2	(5/2) <sup>+</sup>	0.03 0.04							
85	9.271	(3)	(7/2) <sup>-</sup>	0.02 0.03							
86	9.341	0	1/2 <sup>+</sup>	0.02 0.02							
87	9.451	0	1/2 <sup>+</sup>	0.02 0.03							
88	9.545	2	(5/2) <sup>+</sup>	0.05 0.07							
89	9.612										
90	9.678	2	(5/2) <sup>+</sup>	0.04 0.05							
91	9.720	0	1/2 <sup>+</sup>	0.01 0.01							
		+									
		2	(5/2) <sup>+</sup>	0.01 0.01							
92*	9.776	0	1/2 <sup>+</sup>	0.01 0.01							
		+									
		2	(5/2) <sup>+</sup>	0.01 0.02							

Table 6 (continued)

n <sup>o</sup> a)	E <sub>x</sub> <sup>b)</sup> (MeV)	This work			Previous results <sup>e)</sup>					
		ℓ	J <sup>π</sup> c)	C <sup>2</sup> S (SE) (IDP)	E <sub>x</sub> (MeV)	(± keV)	ℓ	(p,d)	C <sup>2</sup> S (d,t)	(τ,α)
93	9.830									
94	9.924									
95	9.978	2	(5/2) <sup>+</sup>	0.06 0.08						
96	10.056	2	(5/2) <sup>+</sup>	0.04 0.06						
97	10.182	2	(5/2) <sup>+</sup>	0.06 0.08						
98	10.238									
99	10.302	2	(5/2) <sup>+</sup>	0.09 0.13						
100	10.358	2	(5/2) <sup>+</sup>	0.09 0.12						
101	10.431	2	(5/2) <sup>+</sup>	0.08 0.11						
102	10.485	2	(5/2) <sup>+</sup>	0.07 0.11						
103	10.581	2	(5/2) <sup>+</sup>	0.07 0.11						
104	10.640	2	(5/2) <sup>+</sup>	0.06 0.09						
105	10.680	2	(5/2) <sup>+</sup>	0.06 0.09						
106*	10.765	0	1/2 <sup>+</sup>	0.07 0.10						
107	11.003	2	(5/2) <sup>+</sup>	0.11 0.16						
108	11.187									
109	11.580									
110	11.826									
111	12.745	0	1/2 <sup>+</sup> ;T=9/2	0.26 0.18	12.737	(5)	0	0.10		
112	13.103	2	3/2 <sup>+</sup> ;T=9/2	0.74 0.46	13.084	(5)	2	0.18		

a) Peaks labelled with an asterisk are doublets.

b) Estimated uncertainties are about 8keV for levels below 6 MeV excitation energy and 10-15 keV for higher lying levels.

c) Value of J<sup>π</sup> assumed in the DWBA calculation. Spin values determined with the CRC analysis (see table 5) are also reported.

d) c.f. discussion in section 4.

e) ref. 1) .

Table 7 : RESULTS OF THE  $^{50}\text{Ti}(\tau,\alpha)^{48}\text{Ti}$  REACTION

n <sup>*</sup>	This work				$^{50}\text{Ti}(\tau,\alpha)^{48}\text{Ti}$ c)			$^{50}\text{Ti}(p,d)^{48}\text{Ti}$ d)			
	E <sub>x</sub> <sup>a)</sup> (MeV)	ℓ	J <sup>π</sup> b)	C <sup>2</sup> S (SE) (IDP)		E <sub>x</sub> (MeV)	ℓ	C <sup>2</sup> S	E <sub>x</sub> (MeV)	ℓ	C <sup>2</sup> S
1	0.0	3	7/2	5.06	6.07	0.0	3	6.04	0.0	3	3.60
2	1.383	(1)	3/2 <sup>-</sup>	0.13	0.14	1.37	1	0.15	1.38	1	0.19
3	1.587	(0)	(1/2 <sup>+</sup> )	0.11	0.13	1.57	(1)	0.41	1.58	(1)	0.07
4	1.610	n.p.u.	CRC:9/2 <sup>-</sup>								
5	1.756	n.p.u.	CRC:5/2 <sup>-</sup>			1.75	1	0.09	1.77	(3)	0.05
6	2.260	3	(7/2) <sup>-</sup>	0.61	0.73	2.26	3	0.57	2.27	3	0.58
7	2.469	3	(7/2) <sup>-</sup>	0.32	0.38	2.47	3	0.42			
8	2.500	0	1/2 <sup>+</sup>	1.01	1.23	2.50	0	0.85	2.50	0	(1.50)
						2.52	3	0.18			
9	2.659	2	3/2 <sup>+</sup>	1.52	1.96	2.66	2	2.31	2.66	2	2.40
10	3.170					3.17			3.17	1	0.08
11	3.429	1	(3/2) <sup>-</sup>	0.04	0.06	3.42	(1)	0.14	3.42	1	0.04
12	3.607	2	(3/2) <sup>+</sup>	0.10	0.13	3.51	(2)	0.25			
13	3.697										
14	3.744	3	(7/2) <sup>-</sup>	0.03	0.04						
15	3.781	3	(7/2) <sup>-</sup>	0.04	0.05	3.76	(3)	0.14	3.84	(3)	0.10
16	4.082	3	(7/2) <sup>-</sup>	0.13	0.16	4.08	(1,3)				
17	4.196	3	(7/2) <sup>-</sup>	0.04	0.05						
18	4.243	3	(7/2) <sup>-</sup>	0.29	0.35	4.24	(2)				
19	4.331	3	(7/2) <sup>-</sup>	0.03	0.03						
20	4.455	0	1/2 <sup>+</sup>	0.06	0.07						
21	4.561	0	1/2 <sup>+</sup>	0.11	0.13						
22	4.770	2	3/2 <sup>+</sup>	0.13	0.17						
23	4.906										
24	6.012	2	3/2 <sup>+</sup>	0.28	0.36						
25	7.329	2	3/2 <sup>+</sup>	0.18	0.23						
26	7.626	2	3/2 <sup>+</sup>	0.15	0.19						
27	8.733	3	7/2 <sup>-</sup> , T=7/2	0.63	0.52	8.74	3	0.68	8.75	3	0.23
									8.89	2	0.48
28	10.972	(0)	(1/2 <sup>+</sup> , T=7/2)	(0.32)	(0.29)	10.97	0	0.40	10.9	0	(0.77)
29	11.110	(2)	(3/2 <sup>+</sup> , T=7/2)	(1.02)	(0.67)	11.10	2	1.06	11.10	2	1.7
									11.70	(1)	1.0

a) Estimated uncertainties are about 10 keV for levels below 6 MeV excitation energy, and 15 keV for higher-lying levels.

b) Value of J<sup>π</sup> assumed in the DWBA calculation. Spin values determined in the CRC analysis for levels excited through double-step processes are also indicated (see table 5).

c) Ref.<sup>36)</sup>

d) Ref.<sup>37)</sup>

Table 8 : RESULTS OF THE  $^{52}\text{Cr}(\tau,\alpha)^{51}\text{Cr}$  REACTION

n° a)	This work					Previous results					
	E <sub>x</sub> <sup>b)</sup> (MeV)	ℓ	J <sup>π</sup> c)	C <sup>2</sup> S		$^{52}\text{Cr}(\text{p,d})^{51}\text{Cr}$ d)			$^{52}\text{Cr}(\tau,\alpha)^{51}\text{Cr}$ e)		
				(SE)	(IDP)	Ex (MeV)	ℓ	C <sup>2</sup> S	Ex (MeV)	ℓ	C <sup>2</sup> S
1	0.0	3	7/2 <sup>-</sup>	5.15	5.88	0.0	3	4.7	0.0	3	5.6
2+3	0.731	1	3/2 <sup>-</sup>	0.07	0.08	0.76	(1)	≤0.07			
4	1.165	n.p.u.	CRC:9/2 <sup>-</sup>			1.173					
5	1.347	3	(5/2) <sup>-</sup>	0.08	0.10	1.364	3	-	1.35	(3)	0.05
6	1.546	3	7/2 <sup>-</sup>	0.03	0.03	1.566	3	-			
7	1.896	n.p.u.				1.907	(1)	≤0.18	1.91	1	0.2
8	2.000	n.p.u.	CRC:5/2 <sup>-</sup>								
9	2.311	3	(7/2) <sup>-</sup>	1.46	1.69	2.319	3	2.0	2.32	3	1.6
10*	2.391										
11	2.699	3	(7/2) <sup>-</sup>	0.03	0.03						
12	2.769	0	1/2 <sup>+</sup>	1.24	1.43	2.789	0	1.3	2.77	0	1.6
13	2.826	1	(3/2) <sup>-</sup>	0.02	0.02						
14	2.914	3	(5/2) <sup>-</sup>	0.05	0.07						
15	2.955	3	(5/2) <sup>-</sup>	0.10	0.12						
16	3.012	2	(3/2) <sup>+</sup>	1.64	1.98	3.034	2	1.5	3.02	2	1.8
17	3.116	1	(3/2) <sup>-</sup>	0.01	0.02						
18	3.349	3	(5/2) <sup>-</sup>	0.07	0.09						
19	3.759	1	(3/2) <sup>-</sup>	0.02	0.03						
20	3.990	2	(3/2) <sup>+</sup>	0.10	0.12						
21	4.079	2	(3/2) <sup>+</sup>	0.23	0.28						
22	4.198	2	(3/2) <sup>+</sup>	0.10	0.12						
23	4.258	2	(3/2) <sup>+</sup>	0.03	0.04						
24	4.359	2	(3/2) <sup>+</sup>	0.07	0.09						
25	4.569	(2)	(3/2) <sup>+</sup>	0.10	0.12						
26	4.583	3	(7/2) <sup>-</sup>	0.06	0.07						
27	4.668	3	(7/2) <sup>-</sup>	0.12	0.14						
28	4.793	(1)	(3/2) <sup>-</sup>	0.13	0.15						
29	4.978	(2)	(3/2) <sup>+</sup>	0.08	0.10						
30	5.030	(2)	(3/2) <sup>+</sup>	0.03	0.03						
		or(3)	or (7/2) <sup>-</sup>	0.02	0.02						
31	5.121	3	(5/2) <sup>-</sup>	0.28	0.33						
32	5.222	1	(3/2) <sup>-</sup>	0.04	0.05						
33	5.265	2	(3/2) <sup>+</sup>	0.17	0.21						
34	5.306	(3)	(7/2) <sup>-</sup>	0.09	0.11						
		or(2)	or (3/2) <sup>+</sup>	0.13	0.16						

Table 8 : RESULTS OF THE  $^{52}\text{Cr}(\tau,\alpha)^{51}\text{Cr}$  REACTION

n <sup>a</sup>	This work				$^{52}\text{Cr}(p,d)^{51}\text{Cr}$ d)			$^{52}\text{Cr}(\tau,\alpha)^{51}\text{Cr}$ e)			
	E <sub>x</sub> (MeV) b)	ℓ	J <sup>π</sup> c)	C <sup>2</sup> S (SE) (IDP)		Ex (MeV)	ℓ	C <sup>2</sup> S	Ex (MeV)	ℓ	C <sup>2</sup> S
35	5.346	(2)	(3/2 <sup>+</sup> )	0.01	0.01						
		or(3)	or(7/2 <sup>-</sup> )	0.05	0.06						
36	5.409	2	(3/2 <sup>+</sup> )	0.04	0.05						
37*	5.455	3	(7/2 <sup>-</sup> )	0.40	0.47						
38	5.537	2	(3/2 <sup>+</sup> )	0.10	0.12						
39	5.761	2	(3/2 <sup>+</sup> )	0.15	0.19						
40	5.832	3	(7/2 <sup>-</sup> )	0.14	0.17						
41	5.943	{0}	(1/2 <sup>+</sup> )	0.09	0.11						
		or(1)	or(3/2 <sup>-</sup> )	0.03	0.03						
42	6.378	2	(3/2 <sup>+</sup> )	0.09	0.11						
43	6.63	3	7/2 <sup>-</sup> , T=5/2	1.11	1.01			6.63	3	1.8	
44	7.31	0	1/2 <sup>+</sup>	0.04	0.05						
45	7.68	0	1/2 <sup>+</sup>	0.05	0.06						
46	7.78	2	(3/2 <sup>+</sup> )	0.14	0.18						
47	8.42	{0}	(1/2 <sup>+</sup> )	0.03	0.03						
48	8.48	0	1/2 <sup>+</sup>	0.04	0.05						
49	9.22	0	1/2 <sup>+</sup> , T=5/2	0.48	0.30			9.19			
50	9.33	2	3/2 <sup>+</sup> , T=5/2	1.17	0.77						

a) Peaks labelled with an asterisk are doublets

b) Uncertainty in excitation energies is about 10 keV for Ex < 6.5 MeV and 20 keV above.

c) Total angular momentum assumed in the DWBA calculation. Spin values determined in the CRC analysis for levels excited through double-step processes are also indicated (see table 5).

d) Ref. <sup>40)</sup>

e) Ref. <sup>41)</sup>





Table 9 continued

n <sup>a)</sup>	E <sub>x</sub> <sup>b)</sup> (MeV)	ℓ	This work			Previous results <sup>a)</sup>					
			J <sup>π</sup> c)	C <sup>2</sup> S		E <sub>x</sub> (MeV)	(± keV)	ℓ	C <sup>2</sup> S	(p,d)	(τ,α)
(SE)	(IDP)										
35	6.418										
36	6.449	2	(3/2) <sup>+</sup>	0.07	0.08						
37	6.528	3	7/2 <sup>-</sup>	0.04	0.05						
38	6.583	1	(3/2 <sup>-</sup> ), T=3/2	0.08	0.06	6.583	(30)	(1)	0.07		
39	6.696	2	(3/2) <sup>+</sup>	0.04	0.05						
40	6.820										
41	6.845										
42	6.958	0	1/2 <sup>+</sup> , T=3/2	0.11	0.07						
43	7.042	0	1/2 <sup>+</sup> , T=3/2	0.62	0.41	7.037	(20)	0	1.0		0.47
44	7.135										
45	7.213	2	(3/2) <sup>+</sup> , T=3/2	0.13	0.09						
46	7.273	2	(3/2) <sup>+</sup> , T=3/2	0.86	0.57	7.267	(20)	2	1.3		0.71
47	7.307	2	(3/2) <sup>+</sup> , T=3/2	0.18	0.12						
48	7.372	2	(3/2) <sup>+</sup> , T=3/2	0.13	0.09						

a) Peaks labelled with an asterisk are doublets.

b) Uncertainty in excitation energies is about 12 keV for  $E_x \leq 4.5$  MeV, 15 keV for  $4.5 \text{ MeV} \leq E_x \leq 6.5$  MeV and 20 keV above.

c) Total angular momentum assumed in the DWBA calculation. Spin values determined in the CRC analysis for levels excited through double-step processes are also indicated (see table 5).

d) See text.

e) Ref. <sup>3)</sup>.

Table 10 : Results of the  $(\tau, \alpha)$  reaction on  $^{40}\text{Ca}$ ,  $^{46}\text{Ti}$  and  $^{50,53,54}\text{Cr}$  target nuclei.

Final nucleus	n <sup>+</sup>	E <sub>x</sub> <sup>a)</sup> (MeV)	l	This work		Previous results c)				
				J <sup>π</sup> · b)	C <sup>2</sup> S		(τ, α)		(p, d)	
					(SE)	(IDP)	l	C <sup>2</sup> S	l	C <sup>2</sup> S
$^{39}\text{Ca}$		0.0	2	3/2 <sup>+</sup>	4.96	4.96	2	3.4	2	4.2
		2.47	0	1/2 <sup>+</sup>	1.74	1.74	0	1.2	0	1.9
		2.78	(3)	7/2 <sup>-</sup>	0.20	0.20	3	1.0	(3)	0.21
		5.13	2	(5/2) <sup>+</sup>	1.52	1.52	2	1.3	2	1.0
		5.49	2	(5/2) <sup>+</sup>	0.67	0.67	(2)		2	0.45
		6.15	2	(5/2) <sup>+</sup>	2.10	2.10	(2)	1.5	2	1.1
$^{47}\text{Ti}$	1	0.0	3	5/2 <sup>-</sup>	0.19	0.22			3	0.12
	2	0.159	3	7/2 <sup>-</sup>	3.22	3.73	3	3.18	3	3.6
	3	1.566(1)		3/2 <sup>-</sup>	0.33	0.37	1	0.26	1	0.15
	4	1.813	2	3/2 <sup>+</sup>	1.51	1.83	2	1.20	2	1.9
	5	2.157	1	(3/2) <sup>-</sup>	0.06	0.07			1	0.03
	6	2.358	0	1/2 <sup>+</sup>	0.78	0.90	0	1.01	0	0.59
	7	2.616	3	(7/2) <sup>-</sup>	0.12	0.14	3	0.17	3	0.29
	8	2.813	3	(5/2) <sup>-</sup>	0.50	0.58	3	0.25	3	0.25
	9	3.220	3	(7/2) <sup>-</sup>	0.48	0.55	3	0.54	3	0.46
	10	7.34	3	7/2 <sup>-</sup> , T=5/2	0.55	0.48	3	0.76	3	0.46
	11	8.14	(2) <sup>d)</sup>	3/2 <sup>+</sup> , T=5/2	1.13	0.79	2	1.19	2	1.4
	12	8.78	(0) <sup>d)</sup>	1/2 <sup>+</sup> , T=5/2	0.36	0.25	0	0.57	0	0.80
$^{49}\text{Cr}$		0.0	3	5/2 <sup>-</sup>	0.12	0.13	(3)	0.19		
		0.268	3	7/2 <sup>-</sup>	3.60	3.93	3	3.8	3	3.4
		2.593	0	1/2 <sup>+</sup>	1.17	1.29	0	1.3		
		3.506	3	7/2 <sup>+</sup>	0.77	0.86	3	0.57		
		4.76	3	7/2 <sup>-</sup> , T=3/2	1.53	1.38	3	1.7		
		5.58	2	3/2 <sup>+</sup>	1.44	0.95	2	2.1		
$^{52}\text{Cr}$		3.418	3	7/2 <sup>+</sup> , (3,4)	1.39	1.62	3	1.3	3	2.3
		3.474	3		1.08	1.26	3	0.96		
		3.774	3	2 <sup>+</sup>	0.31	0.36	3	0.26	3	0.36
		4.017	3		1.03	1.21	3	1.0	3	1.14
		4.605	3		0.19	0.22				
		5.62	(1)		0.49	0.56	1.	0.25		
		5.71	3		0.70	0.83	3	0.72		
		6.18	3		0.48	0.57	(3,1)	(0.25, 0.22)		
		13.55	0	(3,4 <sup>-</sup> ), T=3	0.57	0.37	0	0.39		

Table 10 continued

Final nucleus	n°	This work				Previous results c)				
		E <sub>x</sub> <sup>a)</sup> (MeV)	l	J <sup>π</sup> b)	C <sup>2</sup> S		(τ, α)		(p, d)	
					(SE)	(IDP)	l	C <sup>2</sup> S	l	C <sup>2</sup> S
<sup>53</sup> Cr		1.025	3	(7/2) <sup>-</sup>	0.90	1.08	3	0.49	3	0.51
		1.298	3	(7/2) <sup>-</sup>	0.48	0.58	3	0.45	3	0.70
		1.540	3	(7/2) <sup>-</sup>	3.36	4.04	3	3.0	3	3.2
		3.342	3	(7/2) <sup>-</sup>	1.15	1.40	3	0.93	3	1.2
		3.440	3	(7/2) <sup>-</sup>	0.35	0.43	3	0.37	3	0.30
		4.230	2	(3/2) <sup>+</sup>	0.56	0.74	2	0.22		

- a) Uncertainty on excitation energy is about 20 keV.
- b) Spin and parity assignments in <sup>52</sup>Cr are from ref. 26). For other nuclei, J correspond to the total angular momentum assumed in the DWBA calculation.
- c) previous data given in the tables are from ref. 42) (<sup>39</sup>Ca), ref. 23) (<sup>47</sup>Ti), ref. 32) (<sup>49</sup>Cr), ref. 26) (<sup>52</sup>Cr) and ref. 31) (<sup>53</sup>Cr).
- d) The l-value is from previous work; the C<sup>2</sup>S values are deduced from the cross section at 5° (lab).

Table 11. Coulomb displacement energies  $\Delta E_c$  for the IAS studied in the present work.

n $\ell$ j	Isobar pair	T	$E_x$ (IAS) (keV)	$E_x$ (parent) (keV)	$\Delta E_c$ (keV)	
					this work <sup>a)</sup>	calc. <sup>b)</sup>
1f7/2	<sup>49</sup> Ti - <sup>49</sup> Sc	7/2	8733 ± 15	0.0	7510 ± 17	7402
	<sup>47</sup> Ti - <sup>47</sup> Sc	5/2	7340 ± 20	0.0	7523 ± 21	7524
	<sup>51</sup> Cr - <sup>51</sup> V	5/2	6630 ± 20	0.0	8164 ± 21	8090
	<sup>49</sup> Cr - <sup>49</sup> V	3/2	4760 ± 20	0.0	8111 ± 23	8190
	<sup>53</sup> Fe - <sup>53</sup> Mn	3/2	4262 ± 15	0.0	8791 ± 23	8706
1d3/2	<sup>47</sup> Ca - <sup>47</sup> K	9/2	13103 ± 15	359 ± 6	6888 ± 19	6730
	<sup>49</sup> Ti - <sup>49</sup> Sc	7/2	11110 ± 15	2372.3 ± 0.7	7515 ± 17	7402
	<sup>47</sup> Ti - <sup>47</sup> Sc	5/2	8140 ± 20	767.1 ± 0.4	7556 ± 21	7524
	<sup>51</sup> Cr - <sup>51</sup> V	5/2	9330 ± 20	2675 ± 8	8189 ± 21	8090
	<sup>49</sup> Cr - <sup>49</sup> V	3/2	5580 ± 20	748.1 ± 0.5	8183 ± 23	8190
	<sup>53</sup> Fe - <sup>53</sup> Mn	3/2	7284 ± 20 <sup>c)</sup>	3008 ± 5	8803 ± 23	8706
2s1/2	<sup>47</sup> Ca - <sup>47</sup> K	9/2	12745 ± 15	0.0	6889 ± 19	6730
	<sup>49</sup> Ti - <sup>49</sup> Sc	7/2	10972 ± 15	2229.0 ± 0.7	7520 ± 17	7402
	<sup>47</sup> Ti - <sup>47</sup> Sc	5/2	8780 ± 20	1392 ± 5	7571 ± 21	7524
	<sup>51</sup> Cr - <sup>51</sup> V	5/2	9220 ± 20	2545 ± 8	8206 ± 21	8090
	<sup>53</sup> Fe - <sup>53</sup> Mn	3/2	7029 ± 20 <sup>c)</sup>	2707 ± 4	8849 ± 23	8706

a) Calculated using the binding energies of ref.6).

b) Estimated with the semi-empirical formula given in the text.

c) Centroid energy.

Table 12. Comparison of spectroscopic factors of IAS with those measured for the parent states in proton pick-up experiments.

Isobar pair	n $\ell$ j	E <sub>x</sub> (MeV) IAS	E <sub>x</sub> -E <sub>0</sub> <sup>c)</sup> (MeV)	E <sub>x</sub> (parent) (MeV)	(2T <sub>0</sub> +1)C <sup>2</sup> S <sub>n</sub> <sup>b)</sup>		C <sup>2</sup> S <sub>p</sub> <sup>c)</sup>	C <sup>2</sup> S <sub>p</sub> <sup>d)</sup>
					(SE)	(IDP)		
<sup>47</sup> Ca - <sup>47</sup> K	2s1/2	12.74	0.0	0.0	2.34	1.62	1.39	2
	1d3/2	13.10	0.36	0.37	6.66	4.14	2.95	4
<sup>49</sup> Ti - <sup>49</sup> Sc	1f7/2	8.73	0.0	0.0	4.41	3.64	1.92	2
	2s1/2	10.97	2.24	2.23	(2.24)	(1.54)	2.14	2
	1d3/2	11.11	2.38	2.37	(7.14)	(4.69)	3.39	4
<sup>51</sup> Cr - <sup>51</sup> V	1f7/2	6.63	0.0	0.0	5.55	5.05	3.70	4
	2s1/2	9.22	2.59	2.54	2.40	1.50	1.85	2
	1d3/2	9.33	2.70	2.68	5.85	3.85	3.46	4
<sup>53</sup> Fe - <sup>53</sup> Mn	1f7/2	4.26	0.0	0.0	7.14	6.66	5.93	6
	(2p3/2)	5.54	1.27	1.29	0.12	0.09	0.10	0
	(2p3/2)	6.58	2.32	2.39	0.24	0.18	0.16	0
	2s1/2	7.05 <sup>e)</sup>	2.76	2.70	2.19	1.44	1.97	2
	1d3/2	7.28 <sup>c)</sup>	3.02	3.01	3.90	2.61	3.49	4
<sup>47</sup> Ti - <sup>47</sup> Sc	1f7/2	7.34	0.0	0.0	2.75	2.40	1.93	2
	1d3/2	8.14	0.80	0.80	(5.65)	(3.95)	3.63	4
	2s1/2	8.78	1.44	1.40	(1.80)	(1.25)	2.12	2 <sup>1</sup>
<sup>49</sup> Cr - <sup>49</sup> V	1f7/2	4.76	0.0	0.0	4.59	4.14	2.96	4
	1d3/2	5.58	0.82	0.75	4.32	2.85	0.21	2

a) E<sub>0</sub> is the energy of the ground state analog

b) Spectroscopic factors for the neutron-hole analog states computed using the separation energy (SE) method or the coupled-channel procedure, resulting from the use of an isospin-dependent potential (IDP) in the calculation of form factors. T<sub>0</sub> is the isospin of the target nucleus.

c) Spectroscopic factors for the proton-hole states measured in the (d,τ) reaction<sup>45)</sup> for <sup>47</sup>K, <sup>47,49</sup>Sc, <sup>51</sup>V and <sup>53</sup>Mn, and in the (τ,α) reaction<sup>46)</sup> for <sup>49</sup>V.

d) Shell model predictions.

e) Centroid energies. The spectroscopic factors for the IAS are taken equal to the sum of C<sup>2</sup>S values for individual components.

**Table 13.** Comparison of summed experimental strengths  $\Sigma C^2S$ , for the  $T_2$  levels, with the shell model (SM) sum rule.

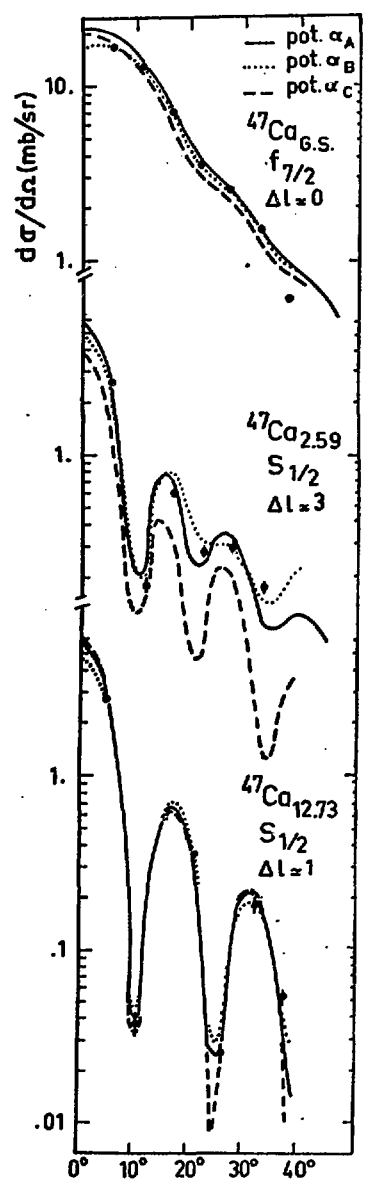
single particle orbital	<sup>47</sup> Ca		<sup>49</sup> Ti		<sup>51</sup> Cr		<sup>53</sup> Fe	
	exp.	SM	exp.	SM	exp.	SM	exp.	SM
1f5/2 <sup>a)</sup>	0.01	0		0	0.7	0	0.06	0
2p3/2	0.04	0	0.2	0	0.2	0	0.2	0
1f7/2	7.4	8	7.7	7.7	8.5	7.2	5.2	6
2s1/2	1.8	1.8	1.4	1.7	1.6	1.6	1.0	1.3
1d3/2	} 5.9	3.5	} 3.0	3.4	} 3.7	3.2	} 1.6	2.7
1d5/2		5.3		5.1		4.8		4

<sup>a)</sup> Only previously known 1f5/2 states have been considered. For all the other  $l=3$  transition, a 1f7/2 transfer has been assumed.

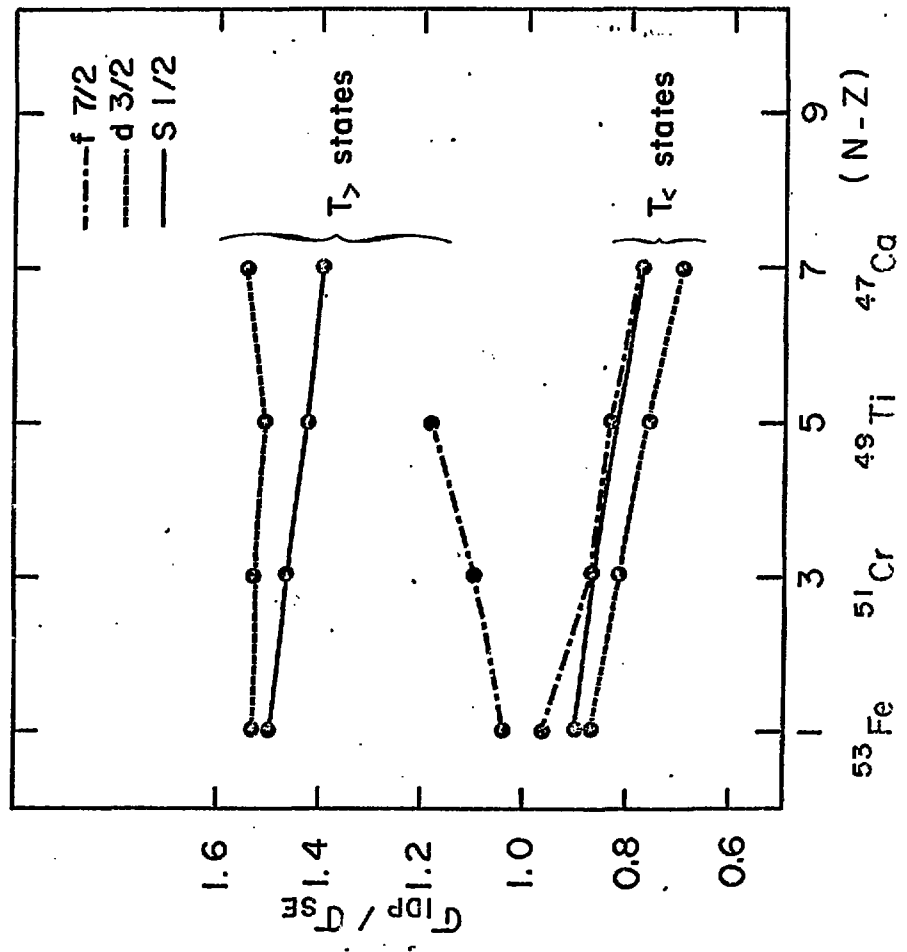
Table 14. Experimental centroid energies (in MeV) of  $T_{<}$  levels.

$n\ell j$	$^{47}\text{Ca}$	$^{49}\text{Ti}$	$^{51}\text{Cr}$	$^{53}\text{Fe}$
$1f7/2$	0.2	0.7	1.01	0.90
$2s1/2$	3.9	2.7	3.4	2.9
$1d3/2^a)$	3.3	3.9	3.6	4.1

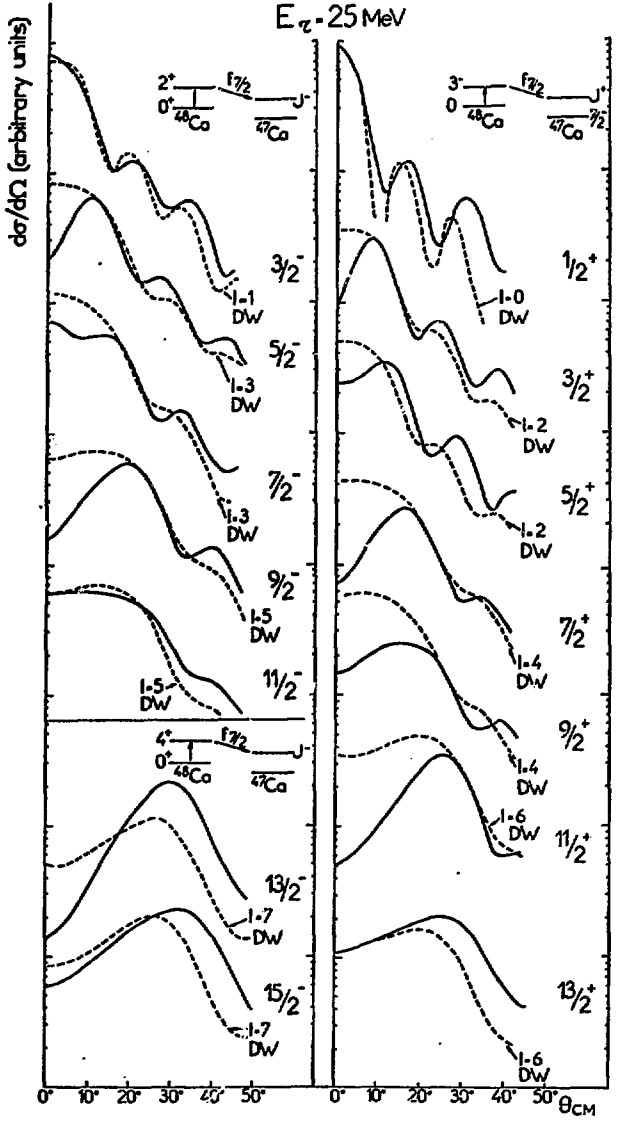
a) In  $^{49}\text{Ti}$  and  $^{53}\text{Fe}$ , centroid energy of all the observed  $\ell=2$  levels. In  $^{47}\text{Ca}$  and  $^{51}\text{Cr}$  the  $1d3/2$   $T_{<}$  sum rule is exhausted at 6.5 MeV and 5.4 MeV respectively and only the levels below these energies have been considered in the estimation of the centroid energy.

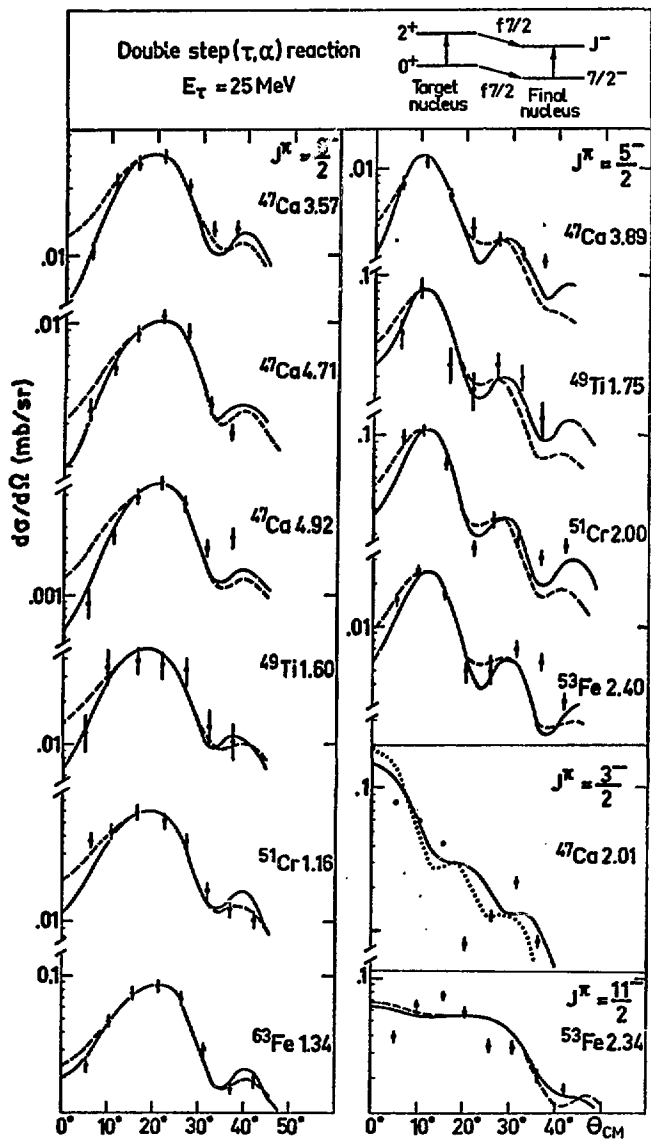


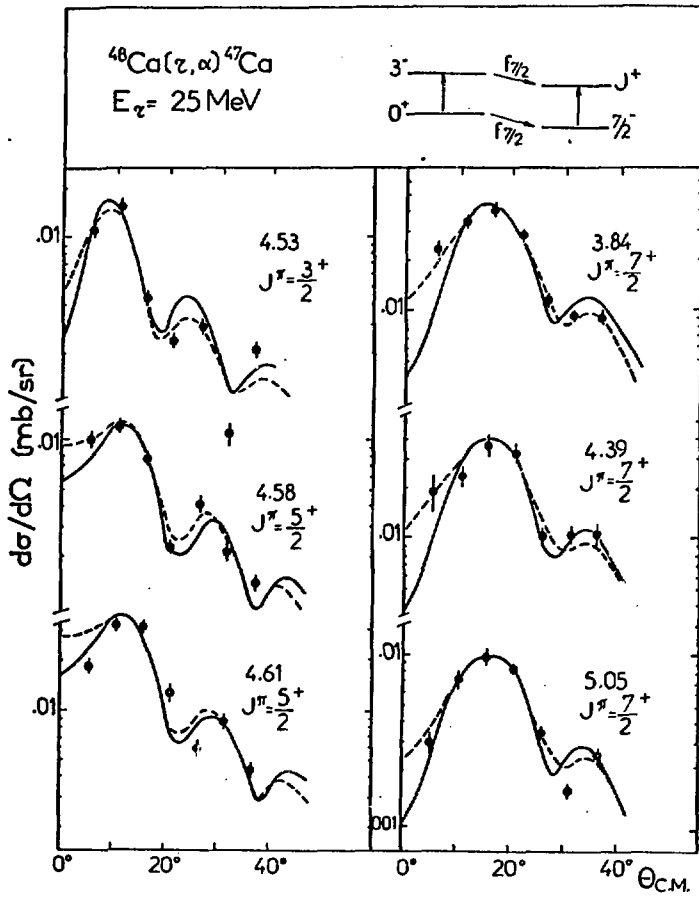


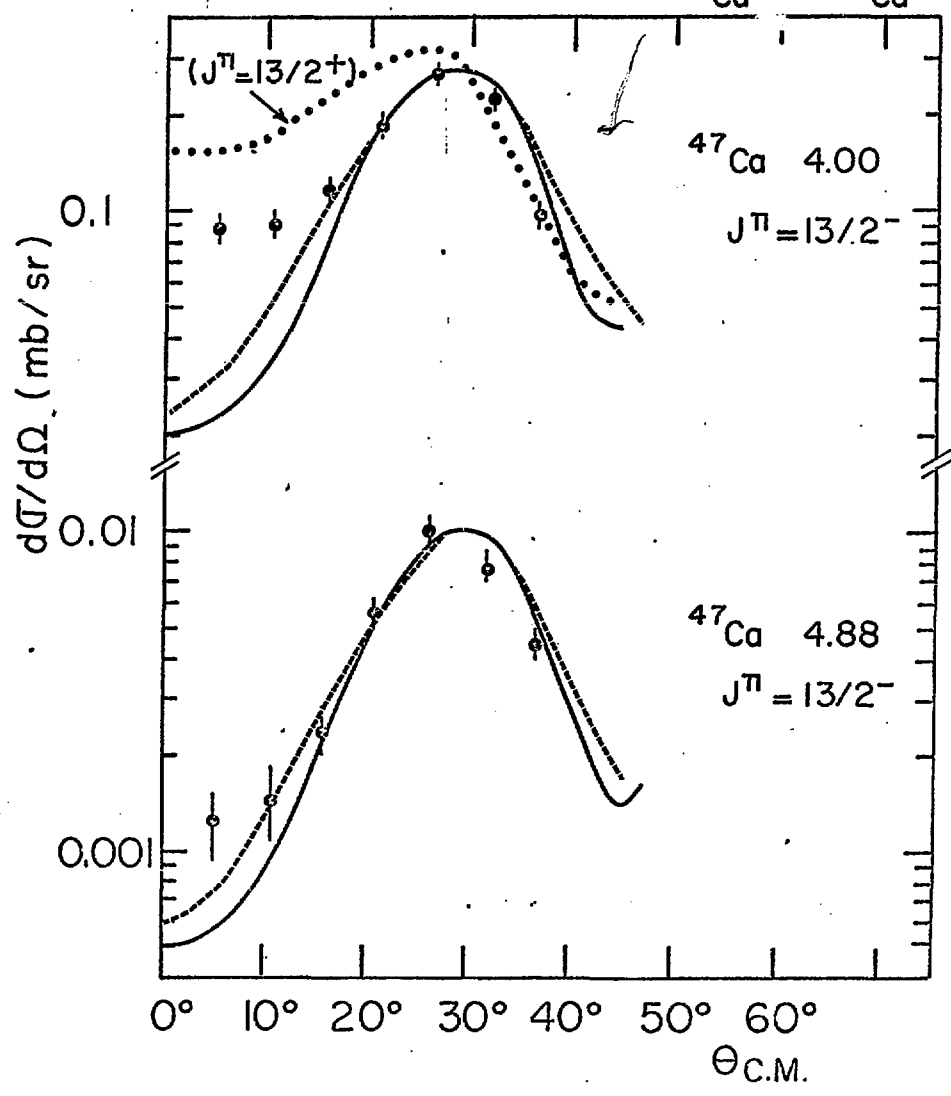
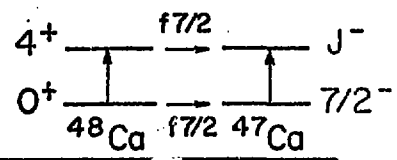
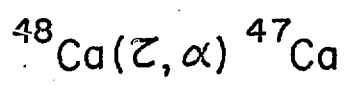


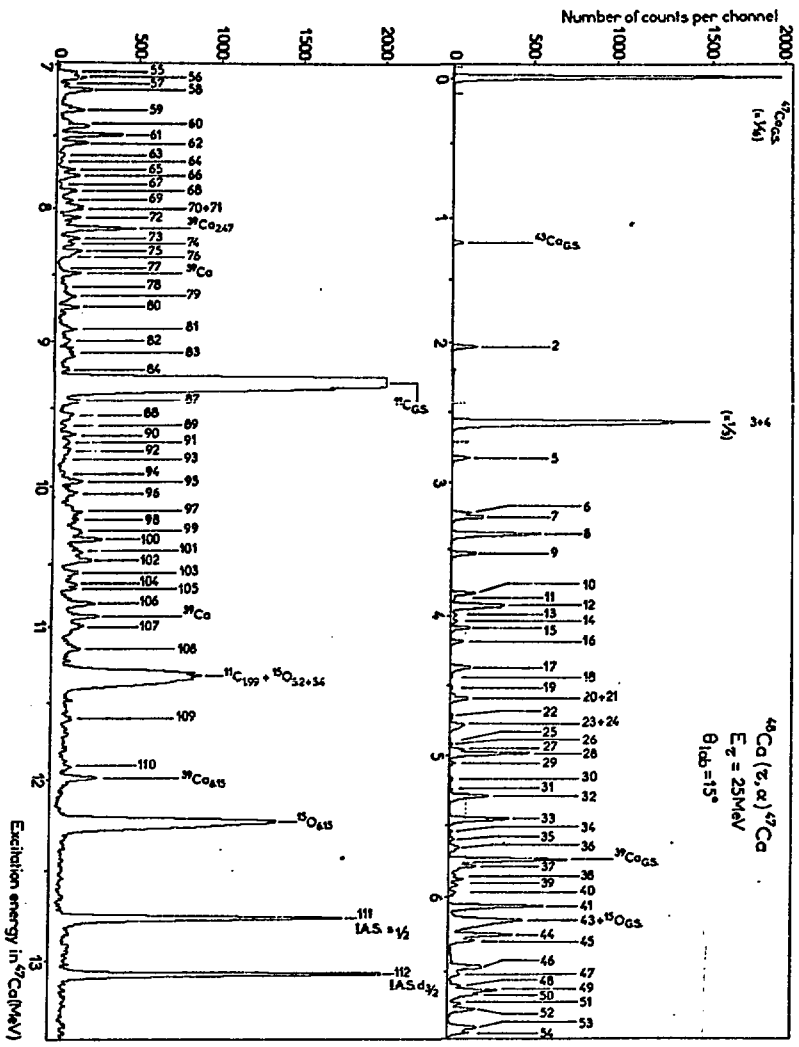
$^{48}\text{Ca}(\tau, \alpha)^{47}\text{Ca}$   
 $E_{\tau} = 25 \text{ MeV}$



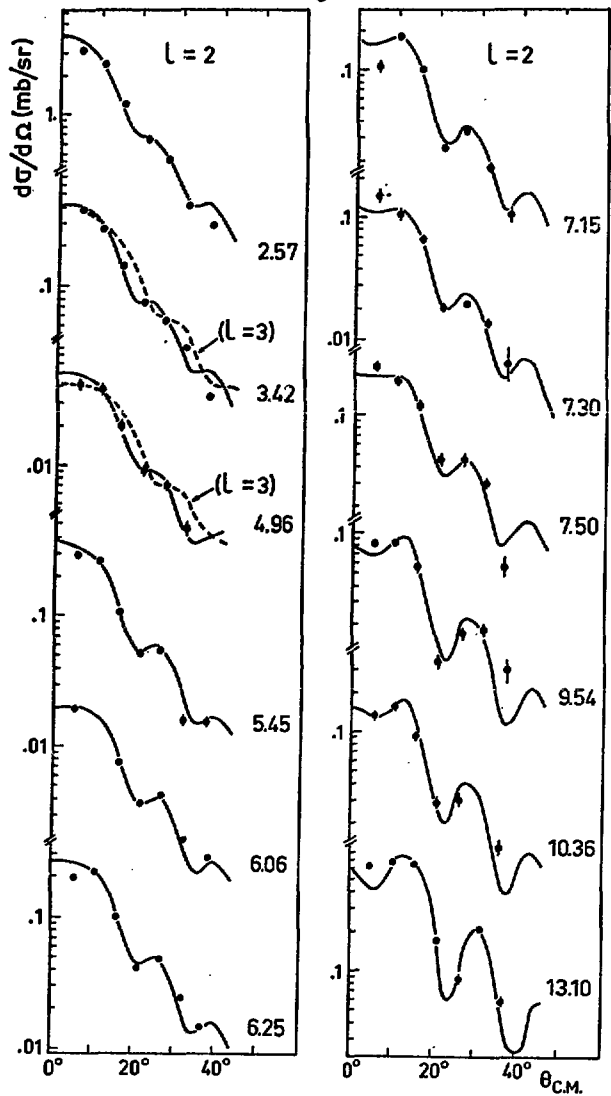




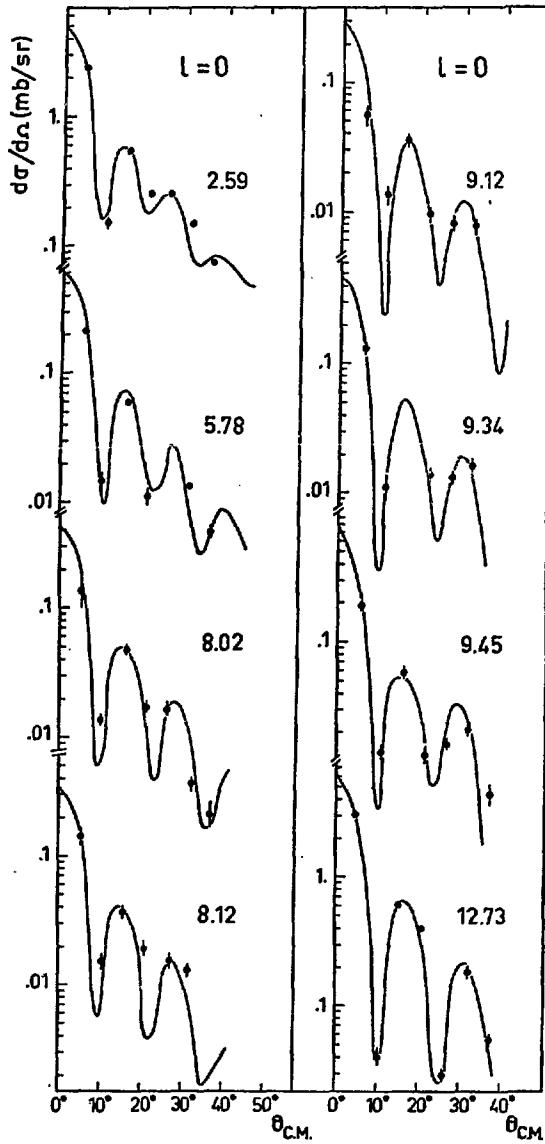




$^{48}\text{Ca}(\tau, \alpha)^{47}\text{Ca}$   
 $E_{\tau} = 25\text{MeV}$

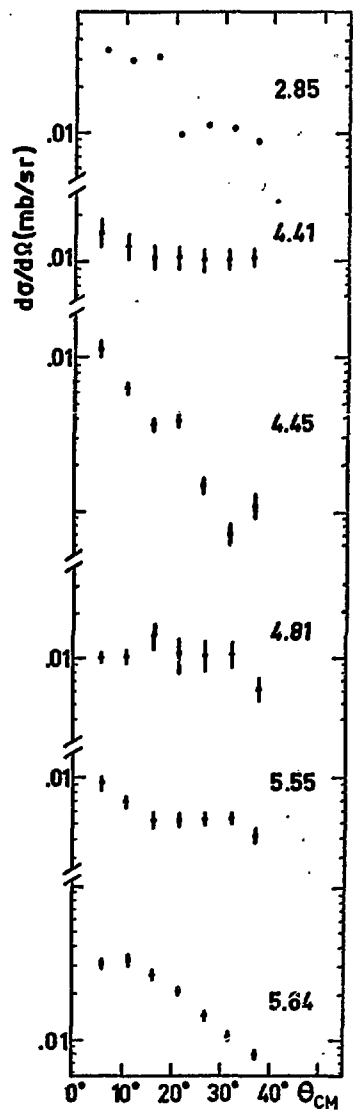


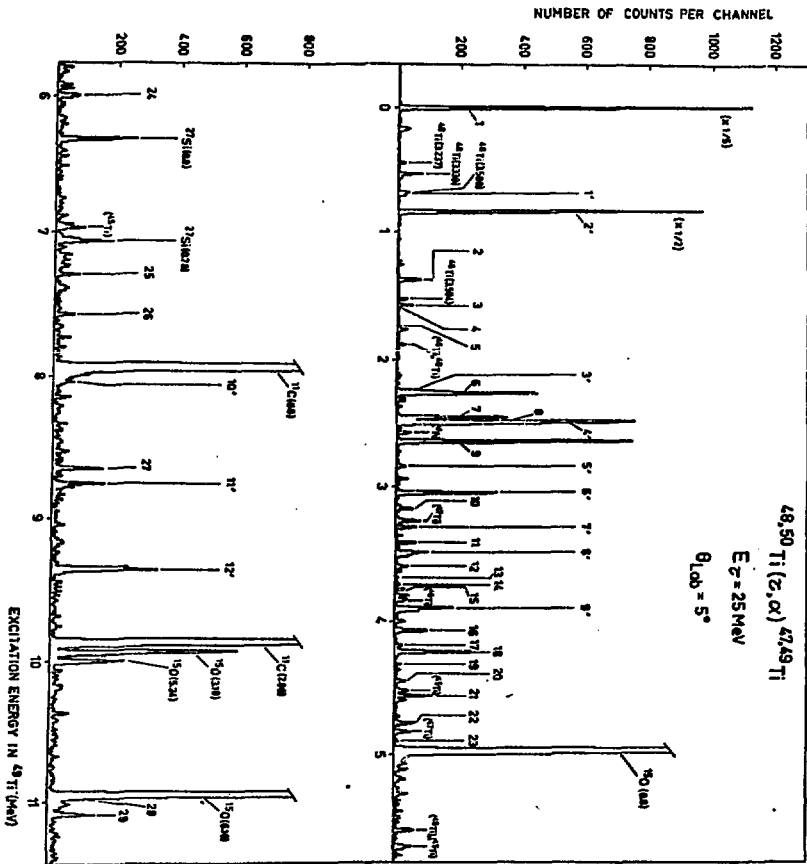
$^{48}\text{Ca}(\tau, \alpha)^{47}\text{Ca}$   
 $E_{\tau} = 25 \text{ MeV}$



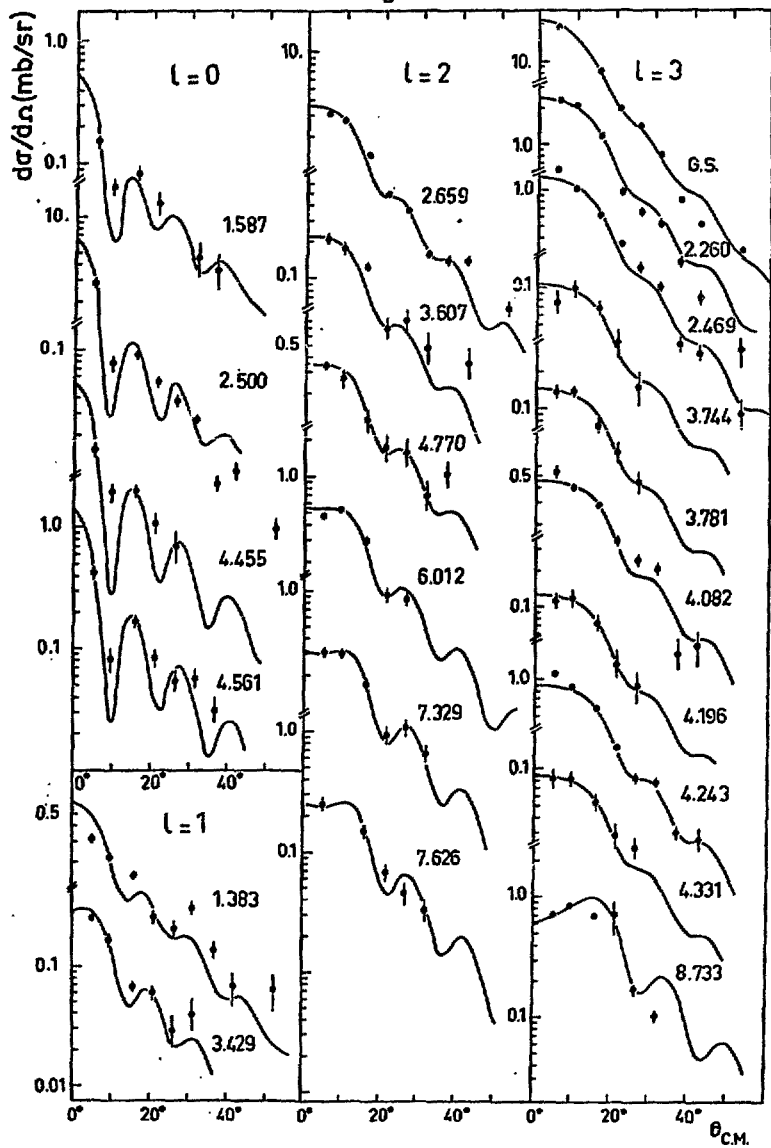


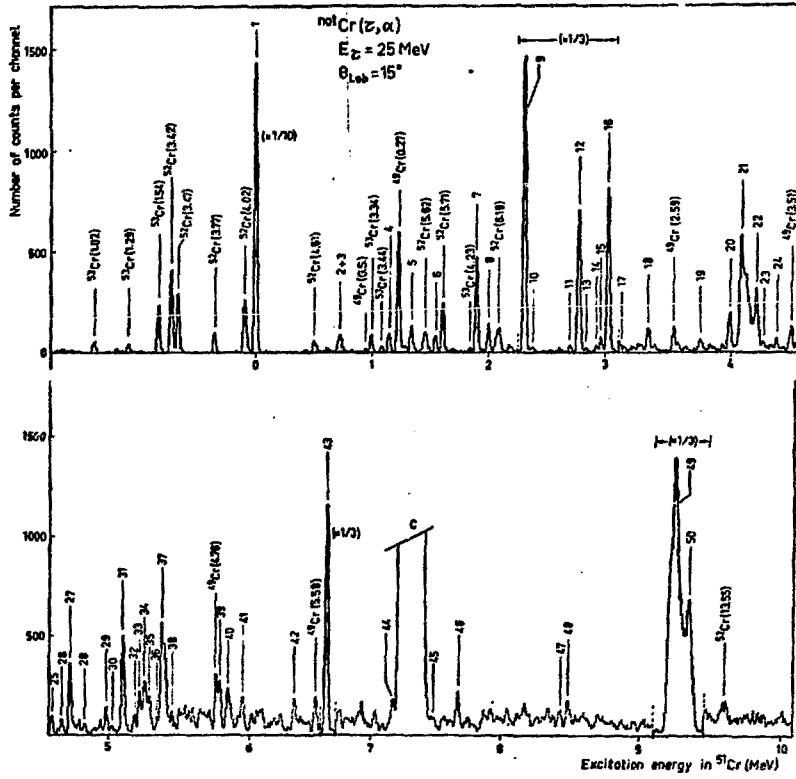
$^{48}\text{Ca}(\tau, \alpha)^{47}\text{Ca}$   
 $E_T = 25 \text{ MeV}$



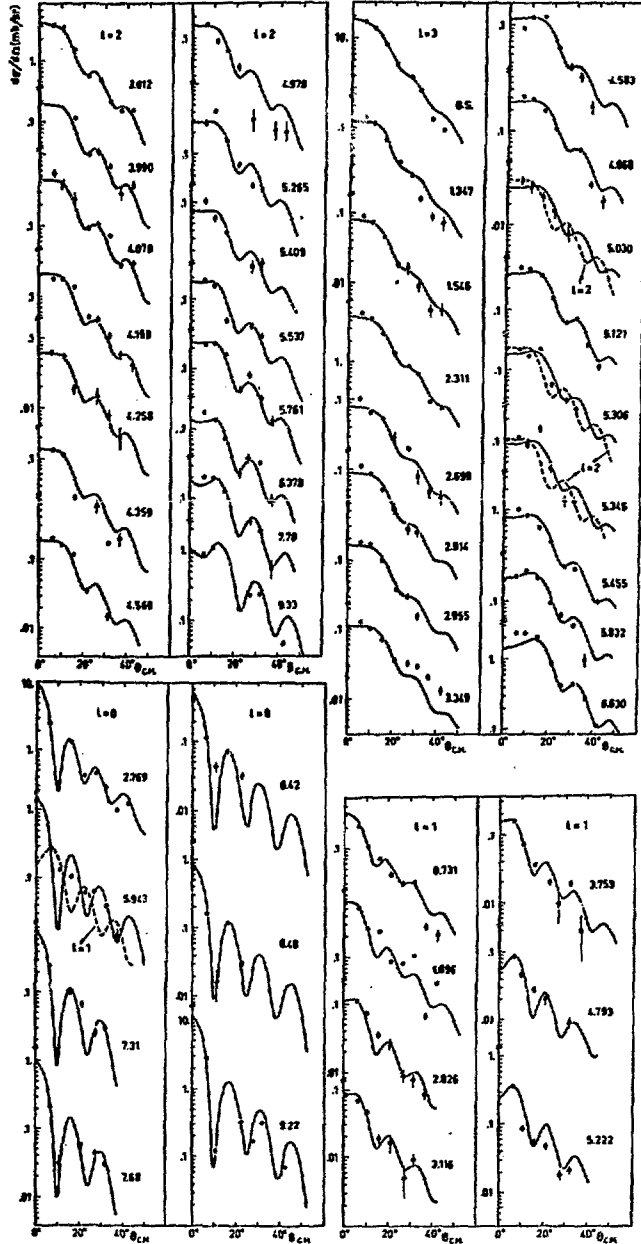


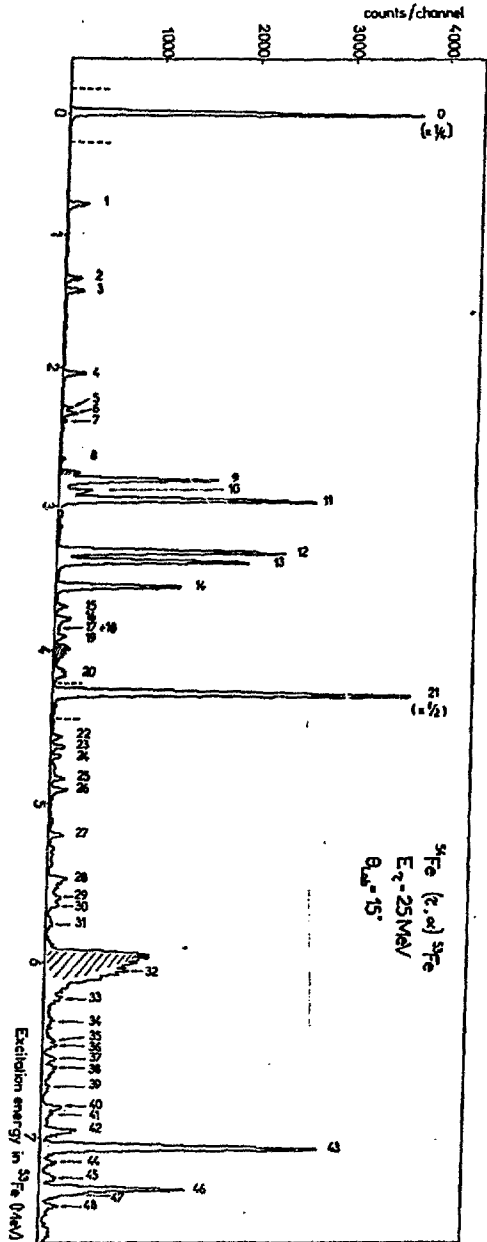
$^{50}\text{Ti}(\tau, \alpha)^{49}\text{Ti}$   
 $E_{\tau} = 25 \text{ MeV}$



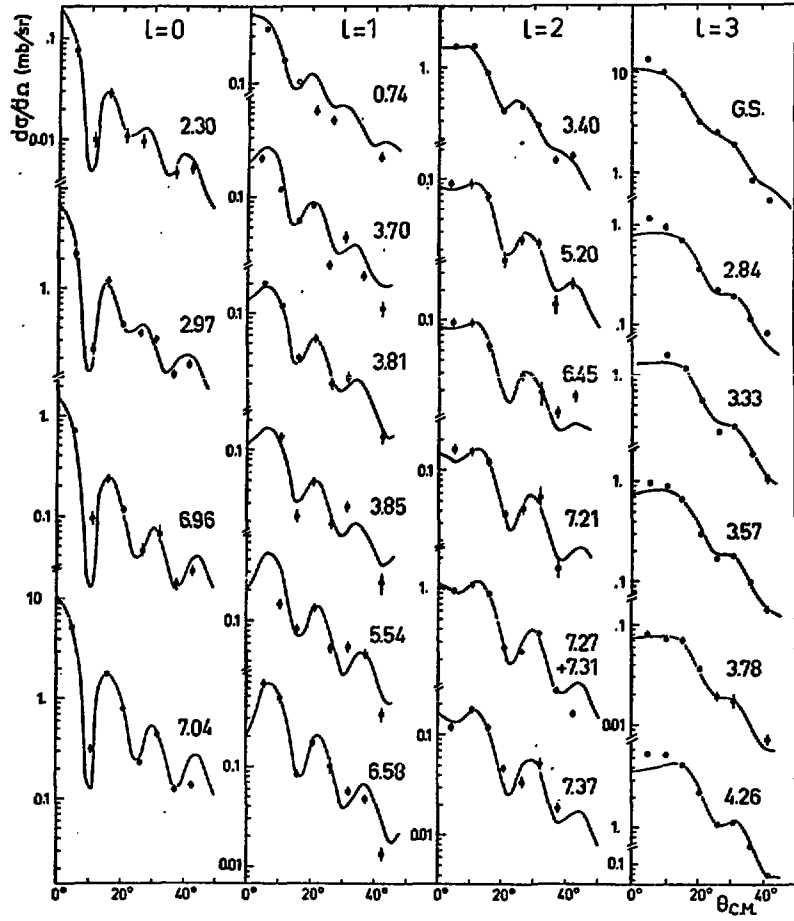


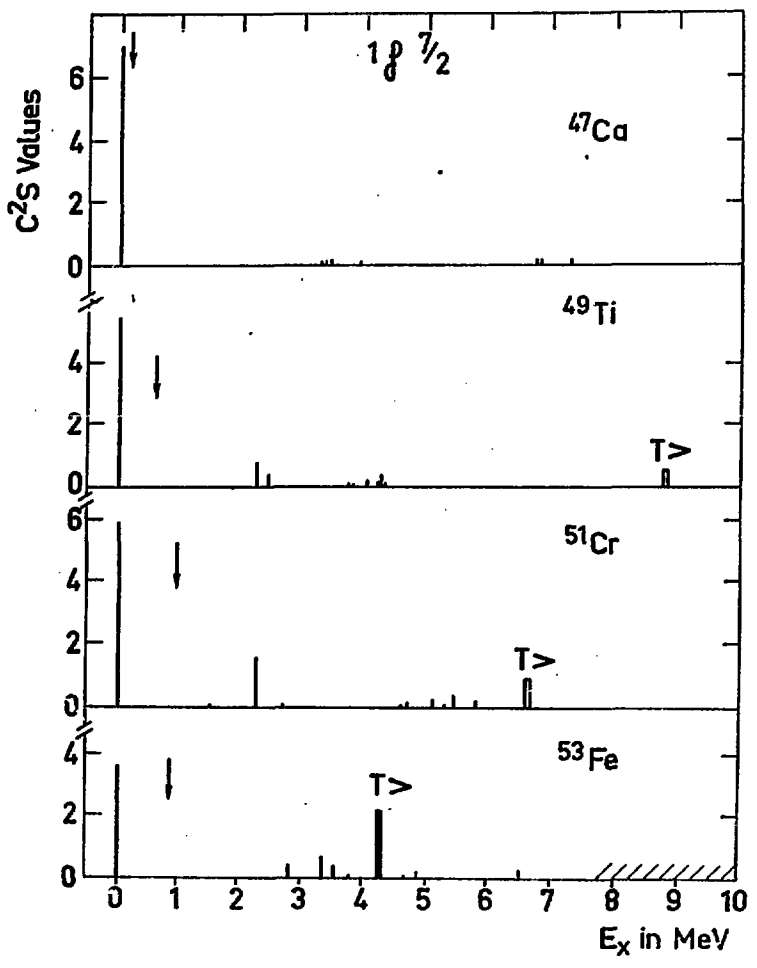
$^{52}\text{Cr}(\alpha, n)^{51}\text{Cr}$   
 $E_\alpha = 25 \text{ MeV}$



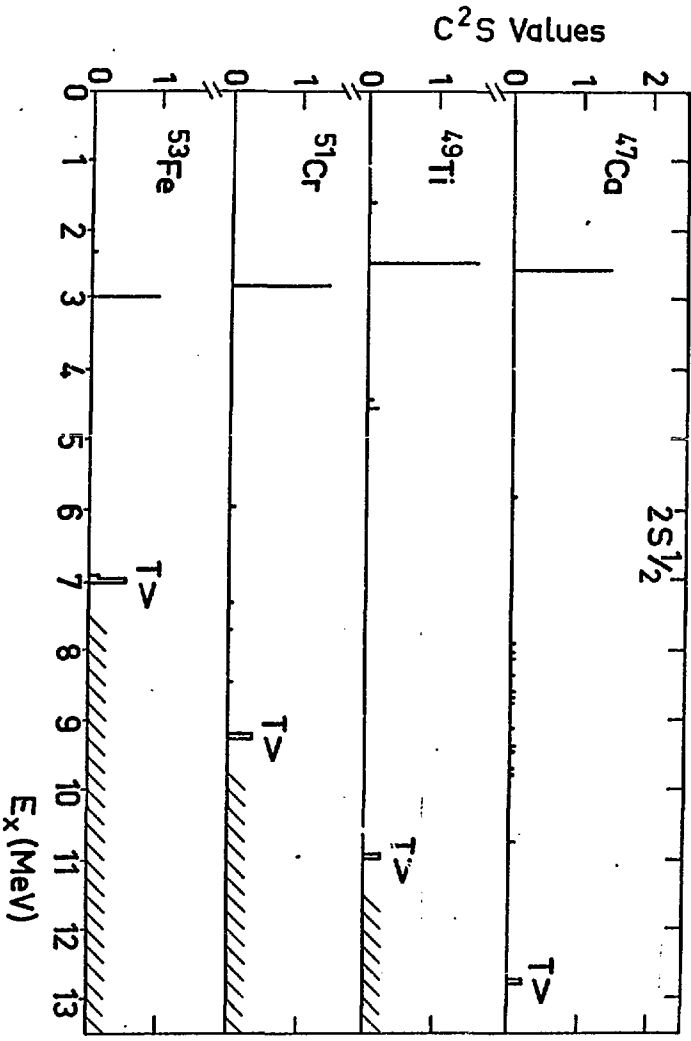


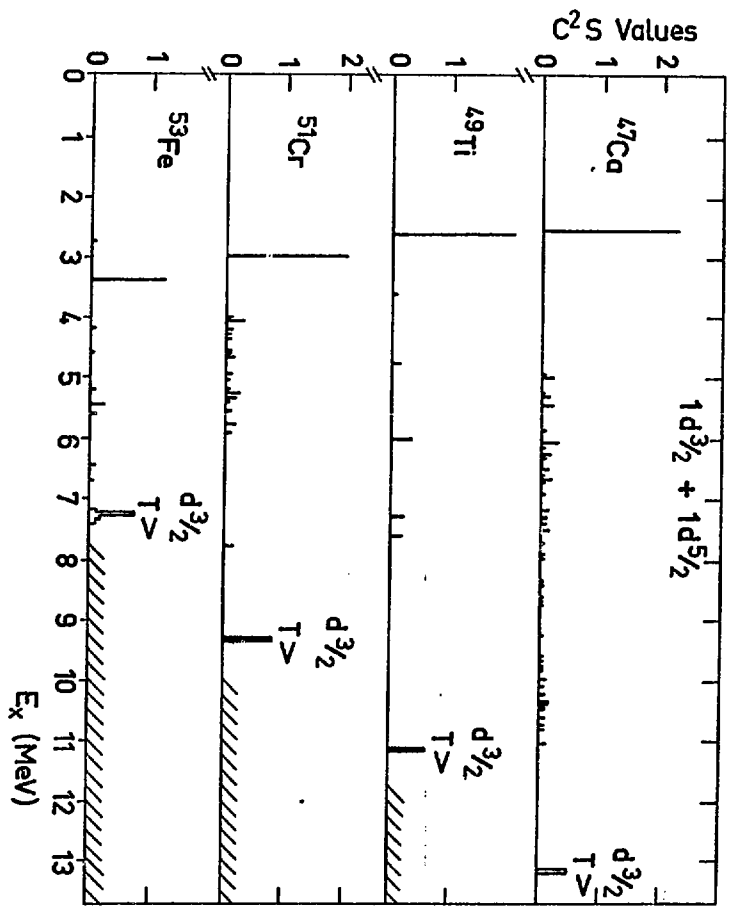
$^{54}\text{Fe}(\tau, \alpha)^{53}\text{Fe}$   
 $E_\tau = 25 \text{ MeV}$



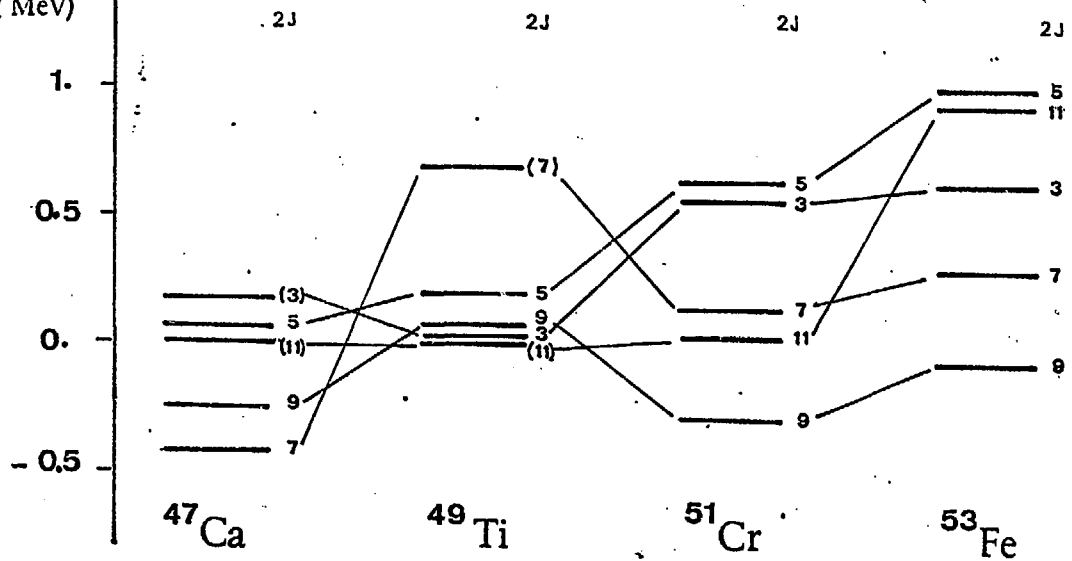








$E_x - E_{2t}$   
(MeV)



中国科学院图书馆